Electronic Supplementary Information (ESI) for the manuscript:

Polymeric iodobismuthates {[Bi_3I_{10}]} and {[BiI_4]} with N-heterocyclic cations: promising perovskite-like photoactive materials for electronic devices

Andrey N.Usoltsev,[a] Moneim Elshobaki,[b,c] Sergey A. Adonin,[a,b,d] Lyubov A. Frolova,[b,e] Tatiyana Derzhavskaya,[e] Pavel A. Abramov,[a,d] Denis V. Anokhin,[e,f,g] Ilya V. Korolkov,[a,d] Sergey Yu. Luchkin,[b] Nadezhda N. Dremova,[e] Keith J. Stevenson,[b] Maxim N. Sokolov,[a,d] Vladimir P. Fedin,[a,d] Pavel A. Troshin[b,e*]

[a] Nikolaev Institute of Inorganic Chemistry, Lavrentieva St. 3, Novosibirsk, Russia

[b] Skolkovo Institute of Science and Technology, 121205 Nobel St. 3, Moscow, Russia

[c] Physics Department, Mansoura University, Mansoura, Egypt,35516

[d] Novosibirsk State University, Pirogova St. 2, Novosibirsk, Russia

[e] Institute for Problems of Chemical Physics RAS, 142432 Academician Semenov St. 1, Chernogolovka, Russia

[f] Faculty for Physicochemical Engineering, Moscow State University, Moscow, Russia

[g] Moscow Institute of Physics and Technology (State University), Institutskiy per. 9, Dolgoprudny, 141700, Russia

Table of contents

Figure 30S. XRD patterns of **3** and **3+I_2** systems 33

X-ray crystallography

Table 1S. Selected geometric parameters in 1-6 (Å)

1		**2**		**3**	
I1—Bi1	3.0880 (7)	I1—Bi1	3.2380 (4)	I4—Bi1^{vi}	3.1482 (6)
I1—Bi2^{i}	3.1603 (7)	I1—Bi1^{v}	3.2380 (4)	I5—Bi3^{vi}	3.4171 (5)
I2—Bi1	3.0623 (6)	I2—Bi1^{v}	3.2526 (4)	I7—Bi3^{vi}	3.1796 (6)
I2—Bi2	3.3967 (8)	I3—Bi1^{v}	3.2638 (4)	I10—Bi3	2.8621 (5)
I2—Bi2^{ii}	3.4113 (8)	Bi1—I2	3.2526 (4)	Bi1—I1	2.8611 (6)
I3—Bi1	3.0881 (6)	Bi1—I3	3.2639 (4)	Bi1—I2	2.8496 (5)
I3—Bi2	3.1145 (8)	Bi1—I4	2.9517 (4)	Bi1—I3	3.0883 (6)
I4—Bi2	2.8543 (8)	Bi1—I5	2.9476 (4)	Bi1—I4^{vii}	3.1482 (6)
I5—Bi2	2.8597 (9)	Bi1—I6	2.9462 (4)	Bi1—I6	3.4192 (5)
Bi1—I1^{iii}	3.0880 (7)			Bi2—I3	3.1098 (5)
Bi1—I2^{iii}	3.0622 (6)			Bi2—I4	3.0331 (5)
Bi1—I3^{iii}	3.0881 (6)			Bi2—I5	3.0993 (6)
Bi2—I1^{iv}	3.1603 (7)			Bi2—I6	3.0578 (5)
Bi2—I2^{ii}	3.4112 (9)			Bi2—I7	3.0454 (5)
				Bi2—I8	3.1418 (5)
				Bi3—I5^{vii}	3.4171 (5)
				Bi3—I6	3.4276 (5)
				Bi3—I7^{vii}	3.1796 (6)
				Bi3—I8	3.0595 (5)
				Bi3—I9	2.8591 (5)
4		**5**		**6**	
I002—Bi01	3.2812 (5)	I1—Bi1	3.0846 (4)	I1—Bi1	3.1299 (6)
I002—Bi01^{v}	3.2812 (5)	I1—Bi1^{viii}	3.2824 (5)	I1—Bi1^{xi}	3.2138 (6)
I003—Bi01	3.2450 (6)	I2—Bi1	2.9027 (5)	I2—Bi1	2.9569 (6)
I003—Bi01^{v}	3.2451 (6)	Bi1—I1^{ix}	3.0846 (5)	I3—Bi1	2.8977 (7)
I004—Bi01	3.2679 (6)	Bi1—I1^{viii}	3.2824 (5)	I4—Bi1	3.0339 (6)
I004—Bi01^{v}	3.2679 (6)	Bi1—I1^{x}	3.2824 (5)	I4—Bi1^{xii}	3.3478 (7)
I005—Bi01	2.9547 (6)	Bi1—I2^{ix}	2.9027 (5)	Bi1—I1^{xi}	3.2138 (6)
I006—Bi01	2.9580 (6)			Bi1—I4^{xii}	3.3479 (7)
I007—Bi01	2.9464 (6)				

Symmetry code(s): (i) x+1/2, y+1/2, z; (ii) -x, -y+1, -z+1; (iii) -x+1/2, -y+3/2, -z+1; (iv) x-1/2, y-1/2, z; (v) x, -y+1/2, z; (vi) x+1, y, z; (vii) x-1, y, z; (viii) -x-1, -y+2, -z+1; (ix) -x-1/2, y, -z+1; (x) x+1/2, -y+2, z; (xi) -x+1, -y+1, -z+1; (xii) -x+2, -y+1, -z+1.

Table 2S. Experimental details

Experiments were carried out at 130 K with Mo *K*α radiation using a New Xcalibur, AtlasS2. Absorption was corrected for by multi-scan methods, *CrysAlis PRO* 1.171.38.41 (Rigaku Oxford Diffraction, 2015) Empirical absorption correction using spherical harmonics, implemented in SCALE3 ABSPACK scaling algorithm.

Parameter	**1**	**2**	**3**	**4**
Chemical formula	$C_6H_8Bi_3I_{10}N$	$C_{18}H_{24}Bi_2I_9N_3$	$C_7H_{10}Bi_3I_{10}N$	$C_{23}H_{33}Bi_2I_9N_4$
M_r	1990.07	1842.46	2004.10	1925.59
Crystal system, space group	Monoclinic, *C*2/*c*	Orthorhombic, *Pnma*	Monoclinic, $P2_1/n$	Orthorhombic, *Pnma*
a, *b*, *c* (Å)	10.8976 (3), 11.2977 (3), 23.3163 (7)	15.5976 (8), 23.0812 (13), 11.0806 (5)	7.6530 (2), 27.2277 (6), 14.2784 (4)	16.4361 (4), 22.9617 (9), 11.2234 (3)
α, β, γ (°)	90, 98.257 (3), 90	90, 90, 90	90, 95.354 (2), 90	90, 90, 90
V (Å^3)	2840.89 (14)	3989.1 (4)	2962.26 (13)	4235.7 (2)
Z	4	4	4	4
μ (mm^{-1})	29.40	15.79	28.20	14.88
Crystal size (mm)	0.20 × 0.15 × 0.05	0.22 × 0.15 × 0.08	0.10 × 0.05 × 0.05	0.20 × 0.08 × 0.05
T_{min}, T_{max}	0.143, 1.000	0.715, 1.000	0.447, 1.000	0.286, 1.000
No. of measured, independent and observed [$I > 2\sigma(I)$] reflections	7228, 3399, 3056	13234, 4797, 4278	15177, 6958, 5735	14012, 5268, 4248
R_{int}	0.091	0.029	0.025	0.047
θ values (°)	θ_{max} = 29.6, θ_{min} = 3.5	θ_{max} = 29.5, θ_{min} = 3.5	θ_{max} = 29.6, θ_{min} = 3.3	θ_{max} = 29.6, θ_{min} = 3.5
$(\sin\theta/\lambda)_{max}$ (Å^{-1})	0.694	0.693	0.694	0.694
Range of *h*, *k*, *l*	$-13 \le h \le 14$, $-15 \le k \le 13$, $-31 \le l \le 26$	$-21 \le h \le 14$, $-29 \le k \le 18$, $-13 \le l \le 14$	$-7 \le h \le 10$, $-37 \le k \le 26$, $-19 \le l \le 19$	$-22 \le h \le 15$, $-19 \le k \le 31$, $-14 \le l \le 8$
$R[F^2 > 2\sigma(F^2)]$, $wR(F^2)$, *S*	0.051, 0.127, 1.07	0.029, 0.064, 1.14	0.030, 0.054, 1.04	0.038, 0.090, 1.06
No. of reflections, parameters, restraints	3399, 94, 0	4797, 154, 0	6958, 190, 0	5268, 179, 0
H-atom treatment	H-atom parameters constrained	H-atom parameters constrained	H-atom parameters constrained	H-atom parameters constrained
	$w = 1/[\sigma^2(F_o^2) + (0.0711P)^2]$ where $P = (F_o^2 + 2F_c^2)/3$	$w = 1/[\sigma^2(F_o^2) + (0.0249P)^2 + 5.1565P]$ where $P = (F_o^2 + 2F_c^2)/3$	$w = 1/[\sigma^2(F_o^2) + (0.0181P)^2]$ where $P = (F_o^2 + 2F_c^2)/3$	$w = 1/[\sigma^2(F_o^2) + (0.0336P)^2 + 18.9353P]$ where $P = (F_o^2 + 2F_c^2)/3$
$\Delta\rho_{max}$, $\Delta\rho_{min}$ (e Å^{-3})	2.78, -4.45	0.93, -1.72	1.38, -1.58	2.29, -4.15

parameter	**5**	**6**
Chemical formula	$C_{10}H_{10}BiI_4N$	$C_{10}H_{10}BiI_4N$
M_r	860.77	860.77
Crystal system, space group	Monoclinic, $I2/a$	Triclinic, $P\bar{1}$
a, b, c (Å)	7.6699 (3), 16.3360 (7), 13.1719 (6)	7.6749 (3), 10.0389 (4), 11.4778 (5)
α, β, γ (°)	90, 91.060 (4), 90	71.809 (4), 84.837 (3), 83.290 (3)
V (Å^3)	1650.10 (12)	833.04 (6)
Z	4	2
μ (mm^{-1})	18.15	17.97
Crystal size (mm)	0.32 × 0.08 × 0.08	0.15 × 0.15 × 0.05
T_{min}, T_{max}	0.174, 1.000	0.139, 1.000
No. of measured, independent and observed [$I > 2\sigma(I)$] reflections	3744, 1942, 1865	6579, 3863, 3419
R_{int}	0.023	0.036
θ values (°)	θ_{max} = 29.4, θ_{min} = 3.9	θ_{max} = 29.6, θ_{min} = 3.3
$(\sin\theta/\lambda)_{max}$ (Å^{-1})	0.691	0.694
Range of h, k, l	$-10 \le h \le 9$, $-22 \le k \le 21$, $-11 \le l \le 18$	$-8 \le h \le 10$, $-11 \le k \le 12$, $-15 \le l \le 15$
$R[F^2 > 2\sigma(F^2)]$, $wR(F^2)$, S	0.032, 0.076, 1.06	0.042, 0.089, 1.03
No. of reflections, parameters, restraints	1942, 88 , 48	3863, 145, 0
H-atom treatment	H-atom parameters not defined	H-atom parameters constrained
	$w = 1/[\sigma^2(F_o^2) + (0.0384P)^2 + 8.281P]$ where $P = (F_o^2 + 2F_c^2)/3$	$w = 1/[\sigma^2(F_o^2) + (0.0375P)^2]$ where $P = (F_o^2 + 2F_c^2)/3$
$\Delta\rho_{max}$, $\Delta\rho_{min}$ (e Å^{-3})	2.84, -2.45	2.83, -4.08

Computer programs: *CrysAlis PRO* 1.171.38.41 (Rigaku OD, 2015), *SHELXS2014* (Sheldrick, 2014), *SHELXL2014* (Sheldrick, 2014), ShelXle (Hübschle, 2011), CIFTAB-2014 (Sheldrick, 2014).

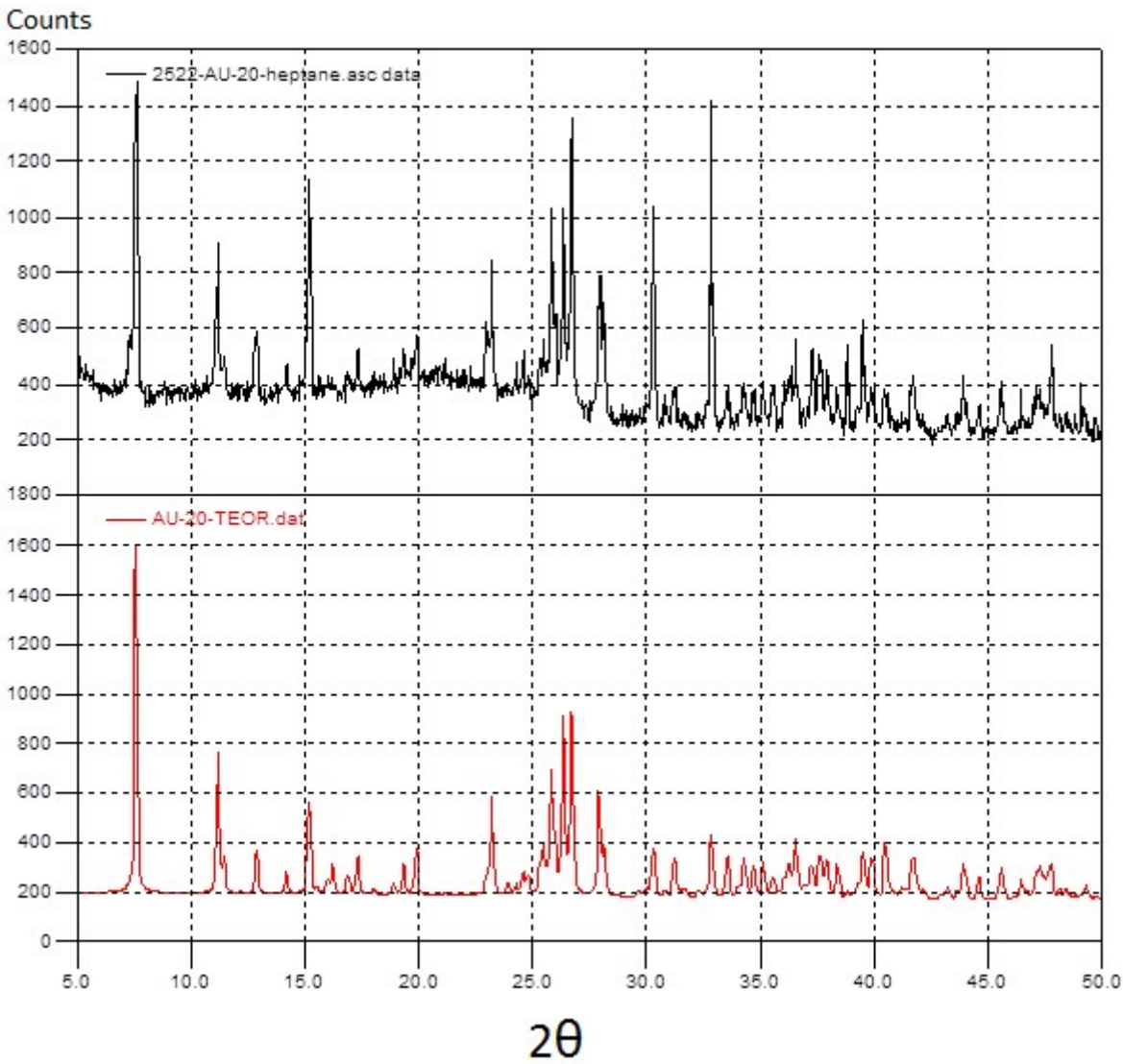

Figure 1S. Powder XRD for the pure phase of **1** (black) shown in comparison with the reference pattern simulated from single crystal x-ray data for this compound (red)

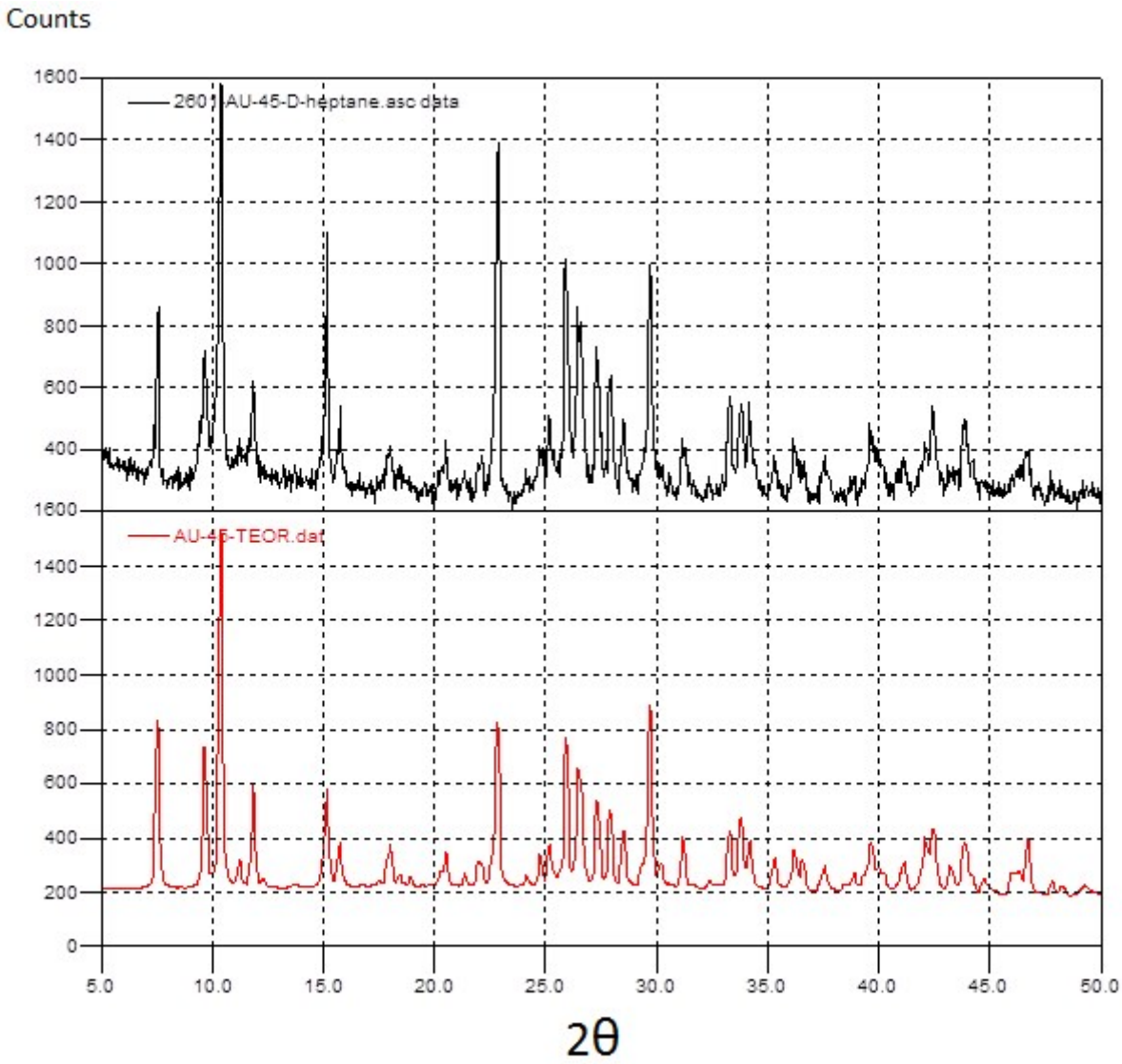

Figure 2S. Powder XRD for the pure phase of **2** (black) shown in comparison with the reference pattern simulated from single crystal x-ray data for this compound (red)

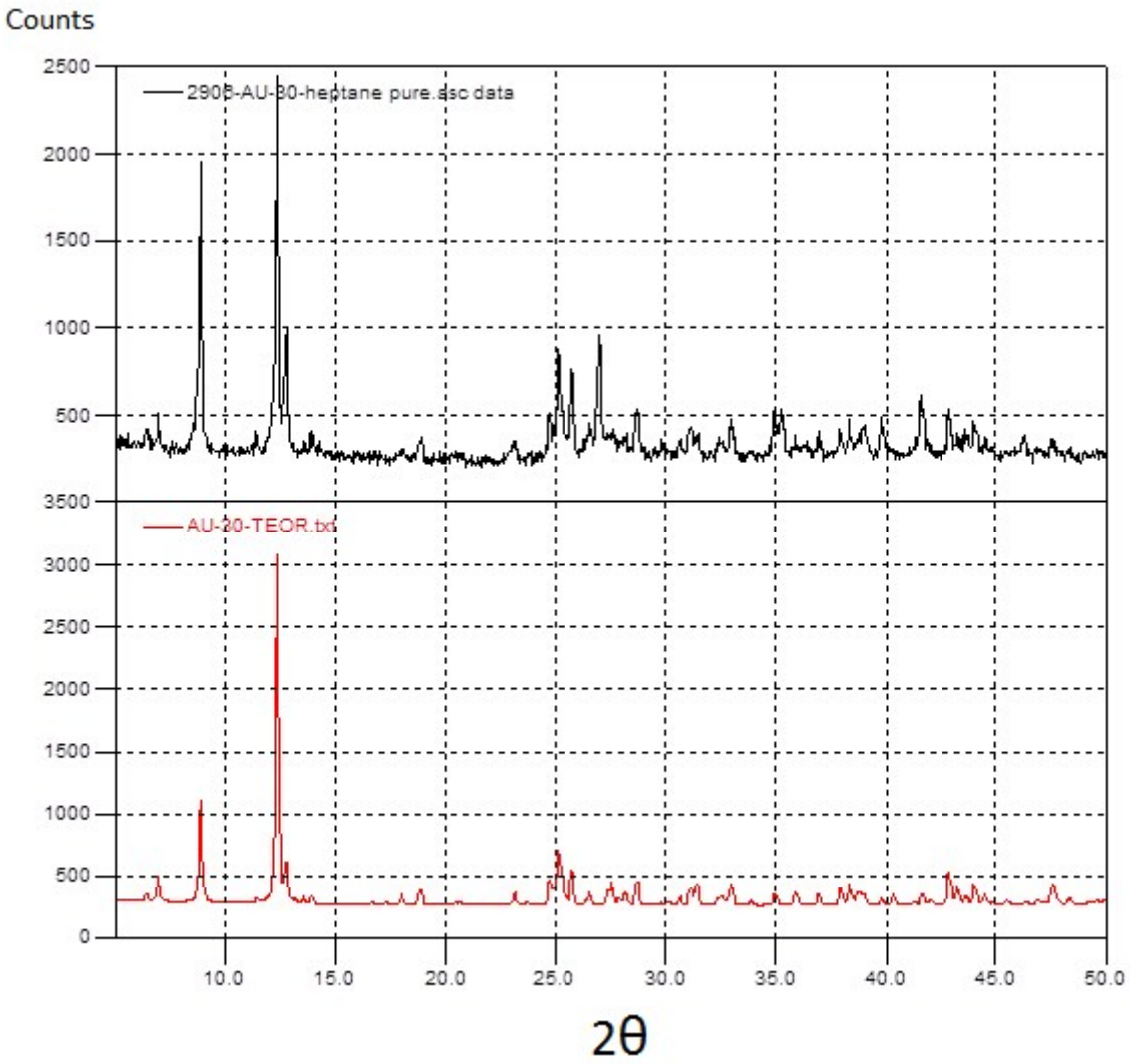

Figure 3S. Powder XRD for the pure phase of **3** (black) shown in comparison with the reference pattern simulated from single crystal x-ray data for this compound (red)

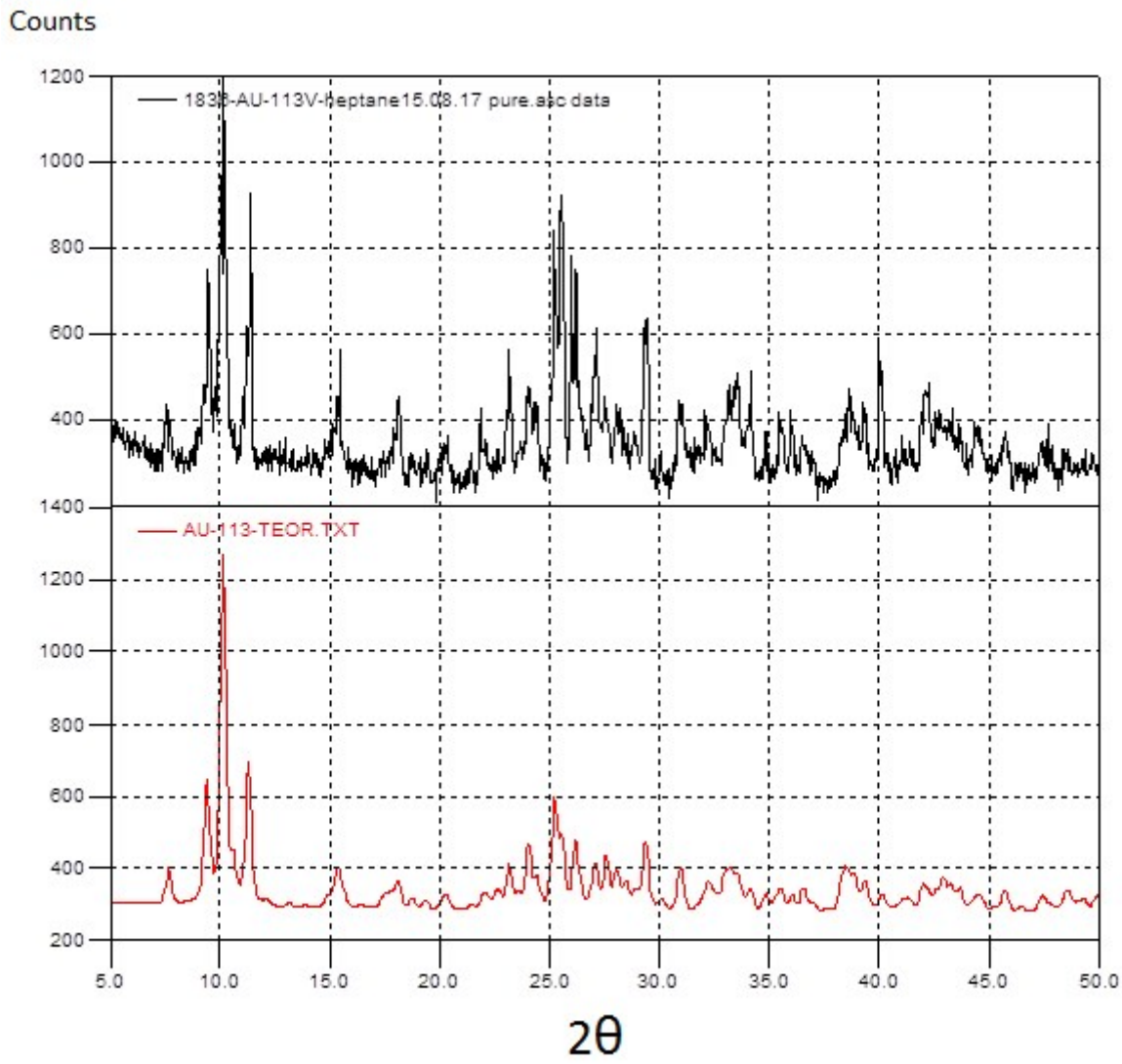

Figure 4S. Powder XRD for the pure phase of **4** (black) shown in comparison with the reference pattern simulated from single crystal x-ray data for this compound (red)

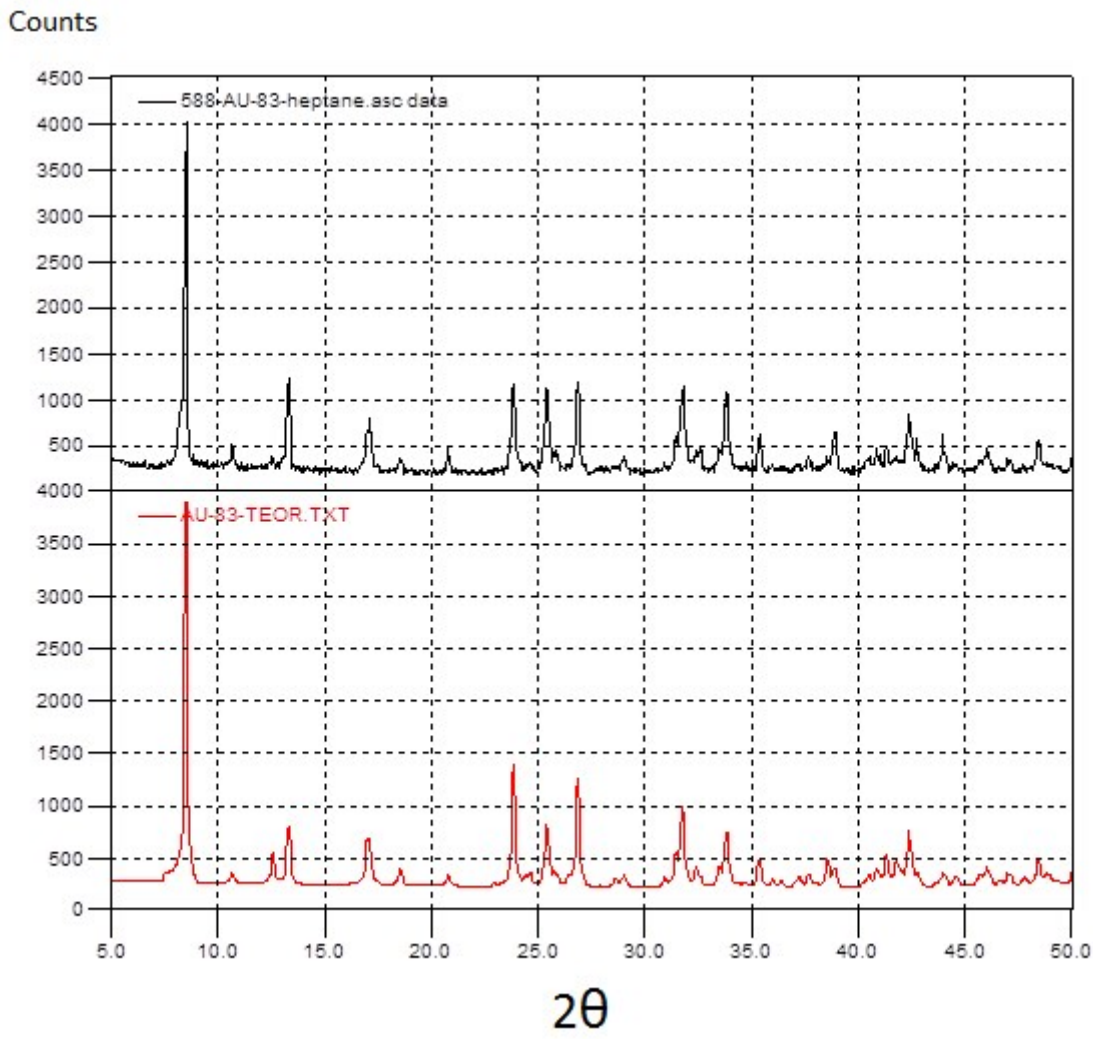

Figure 5S. Powder XRD for the pure phase of **5** (black) shown in comparison with the reference pattern simulated from single crystal x-ray data for this compound (red)

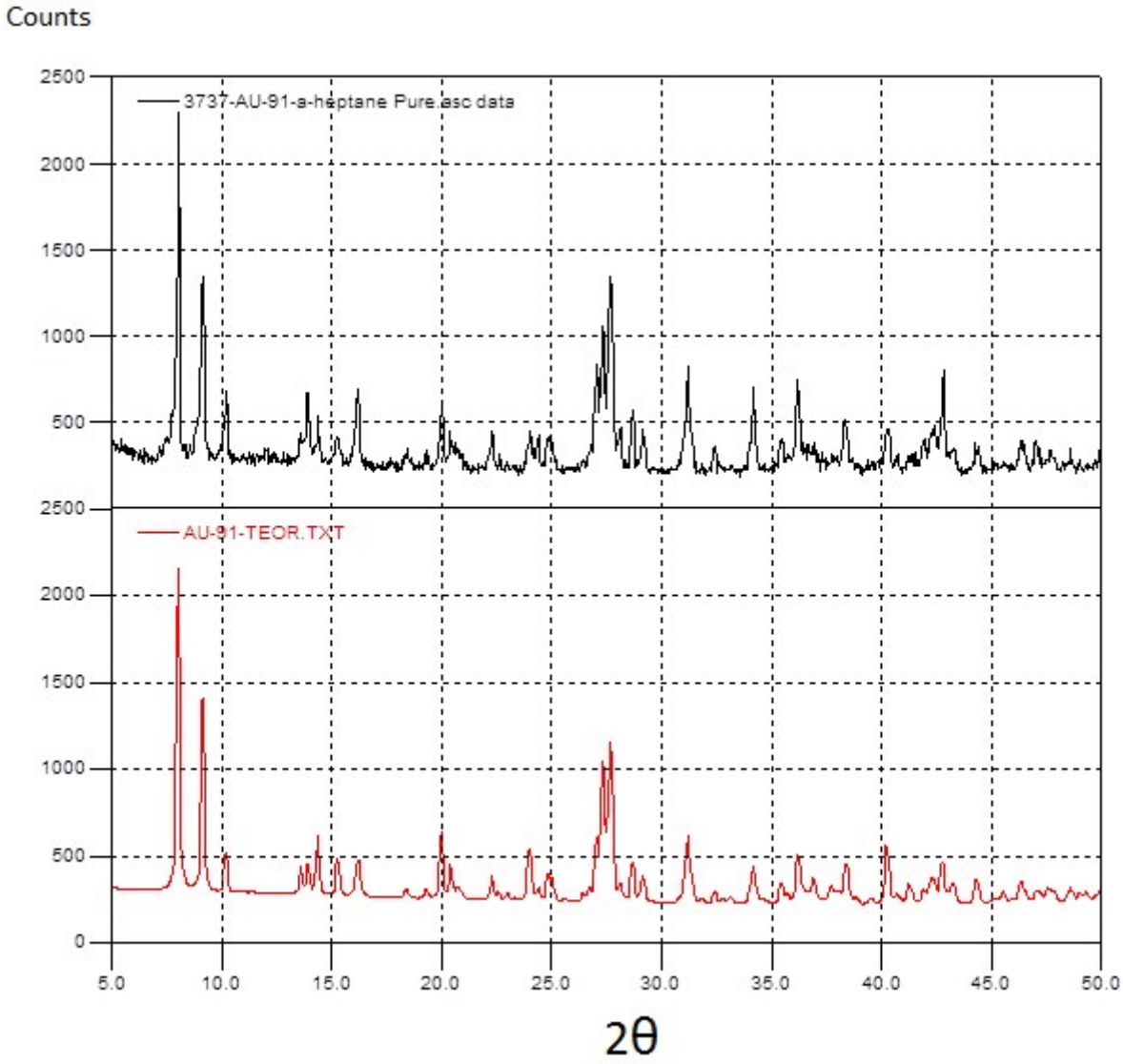

Figure 6S. Powder XRD for the pure phase of **6** (black) shown in comparison with the reference pattern simulated from single crystal x-ray data for this compound (red)

Diffuse reflectance spectra

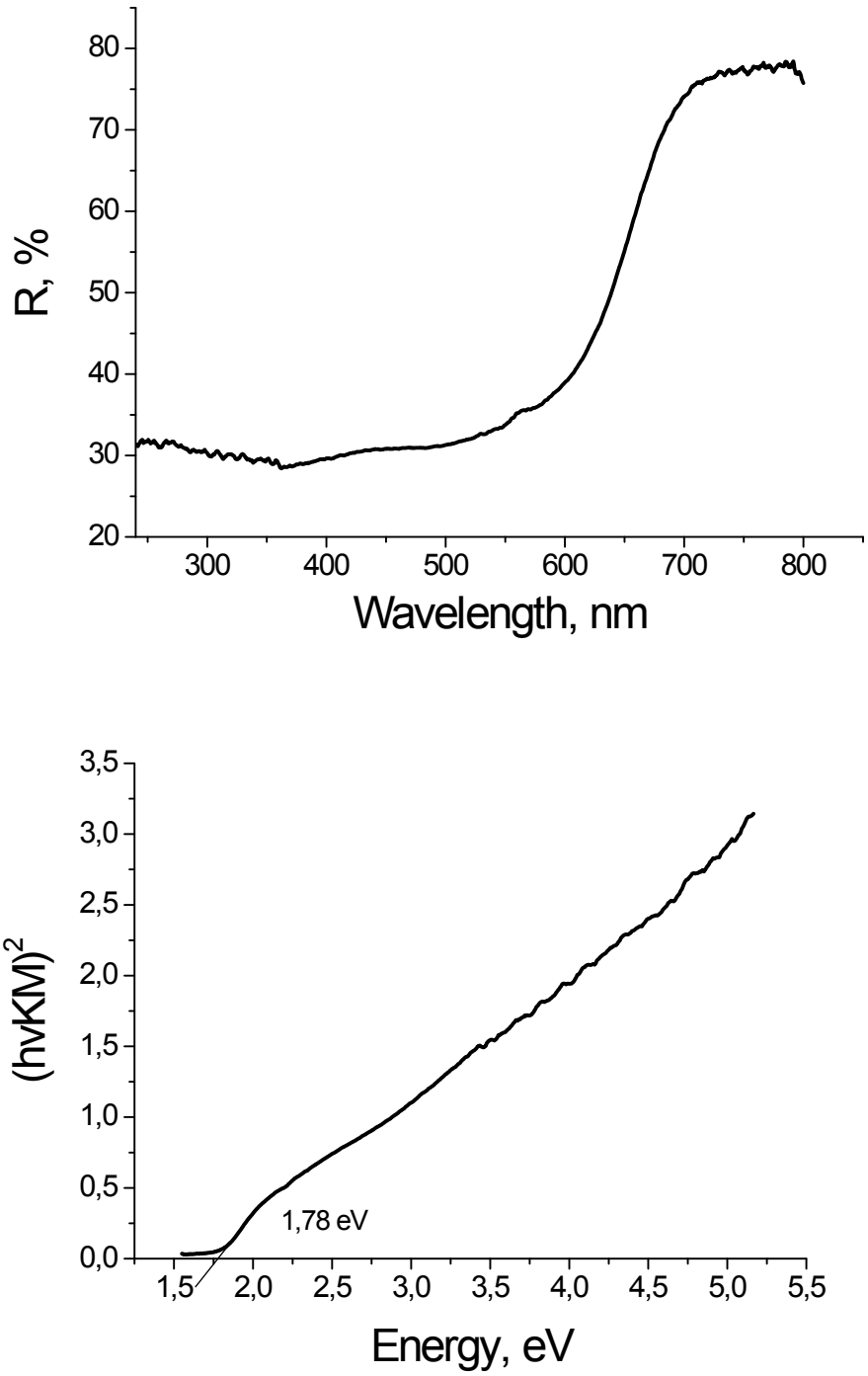

Figure 7S. Diffuse reflectance spectrum (above) and dependence of $(hvKM)^2$ (below) on the incident radiation energy for **1**

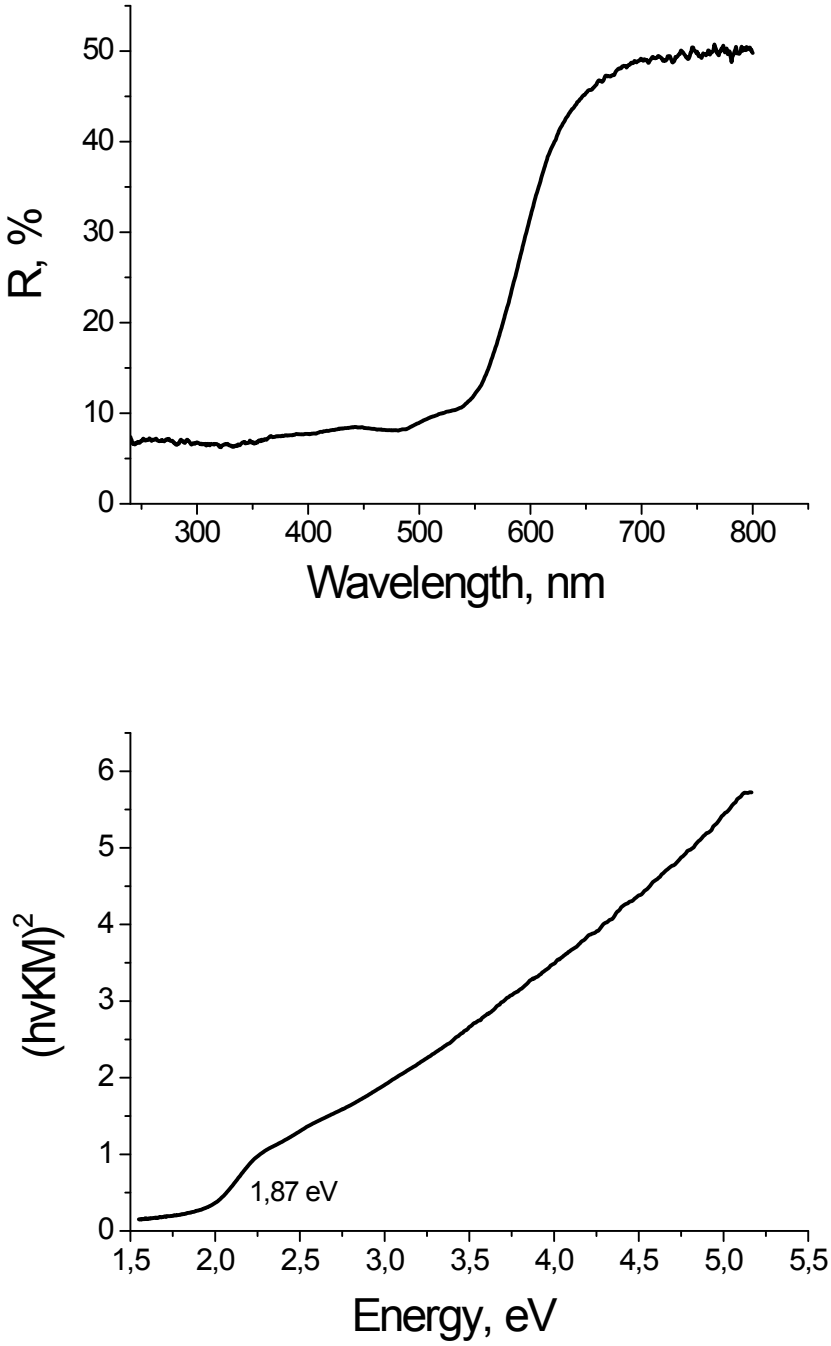

Figure 8S. Diffuse reflectance spectrum (above) and dependence of $(hvKM)^2$ (below) on the incident radiation energy for **2**

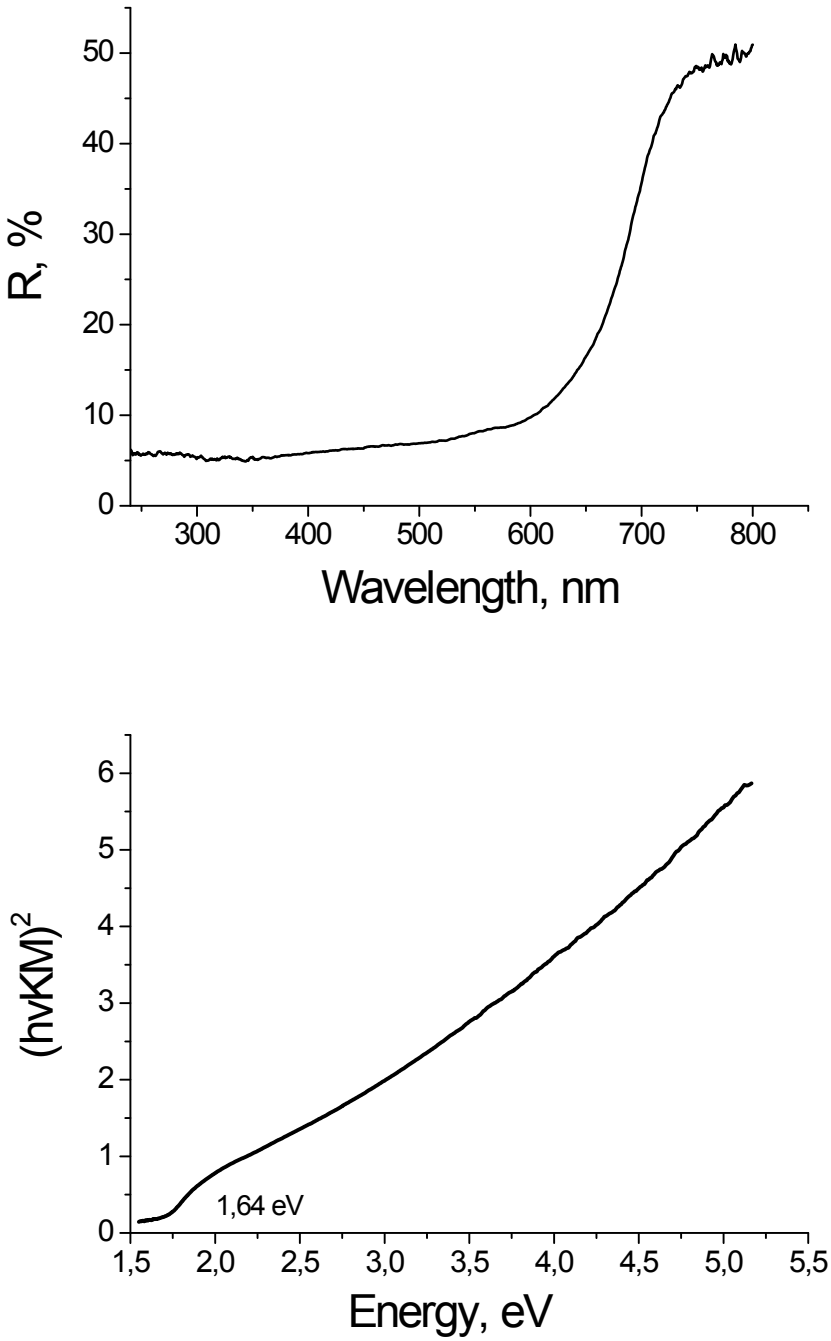

Figure 9S. Diffuse reflectance spectrum (above) and dependence of $(hvKM)^2$ (below) on the incident radiation energy for **3**

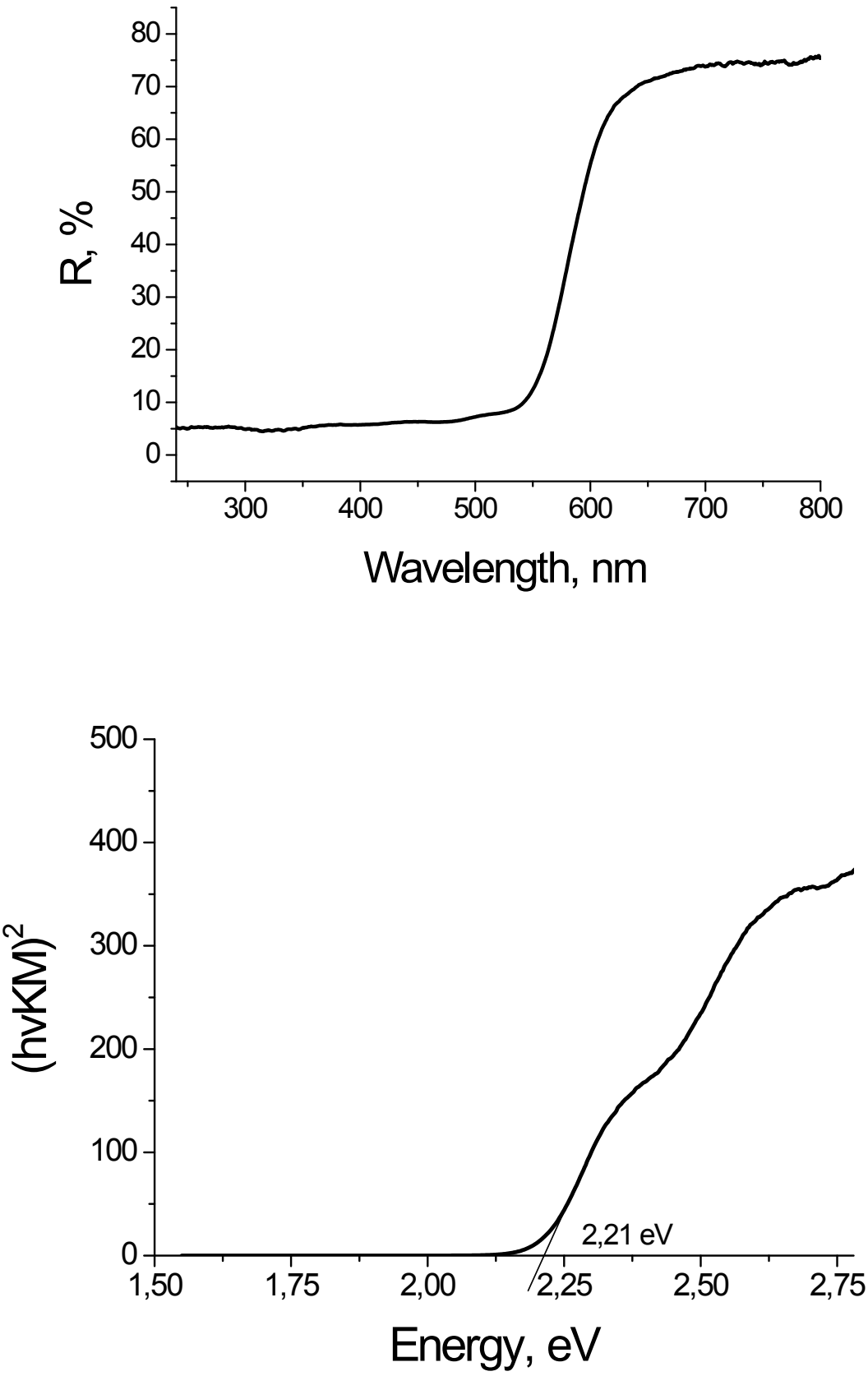

Figure 10S. Diffuse reflectance spectrum (above) and dependence of $(h\nu KM)^2$ (below) on the incident radiation energy for **4**

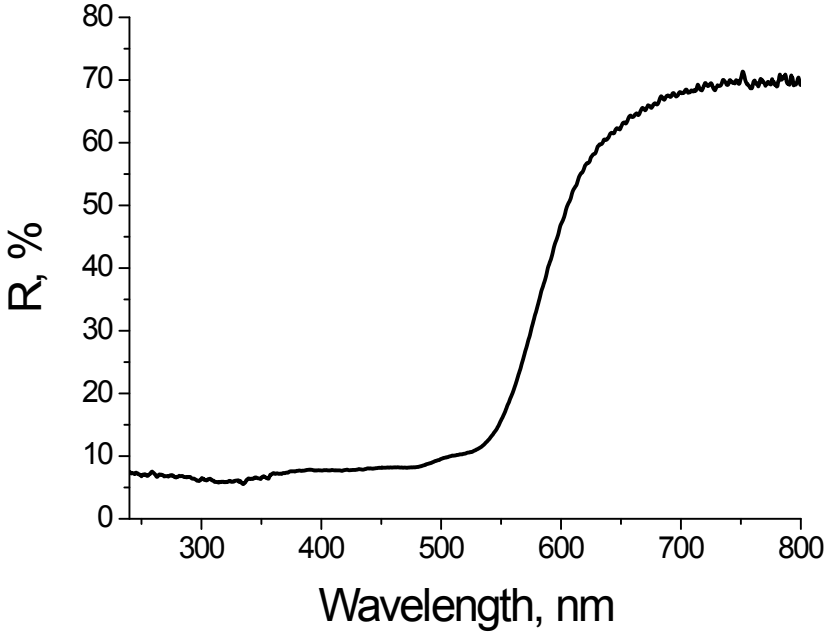

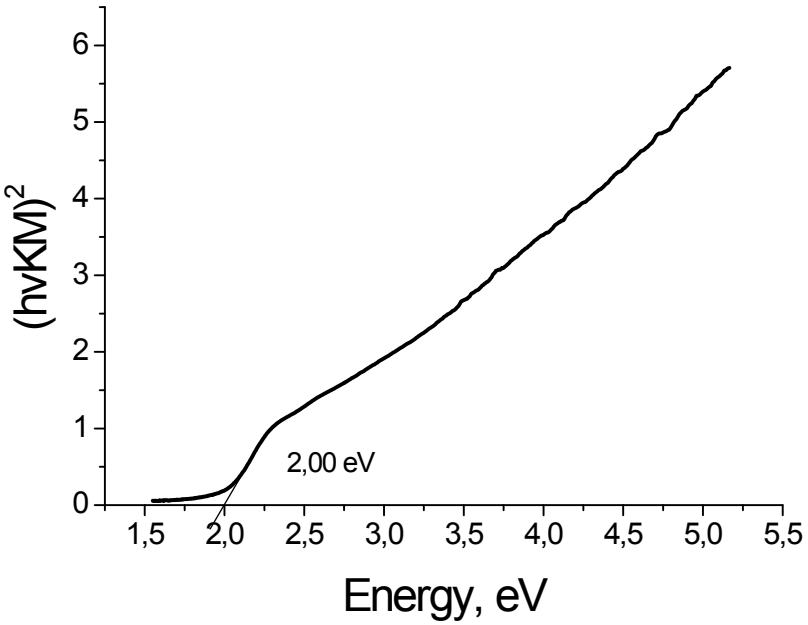

Figure 11S. Diffuse reflectance spectrum (above) and dependence of $(h\nu KM)^2$ (below) on the incident radiation energy for **5**

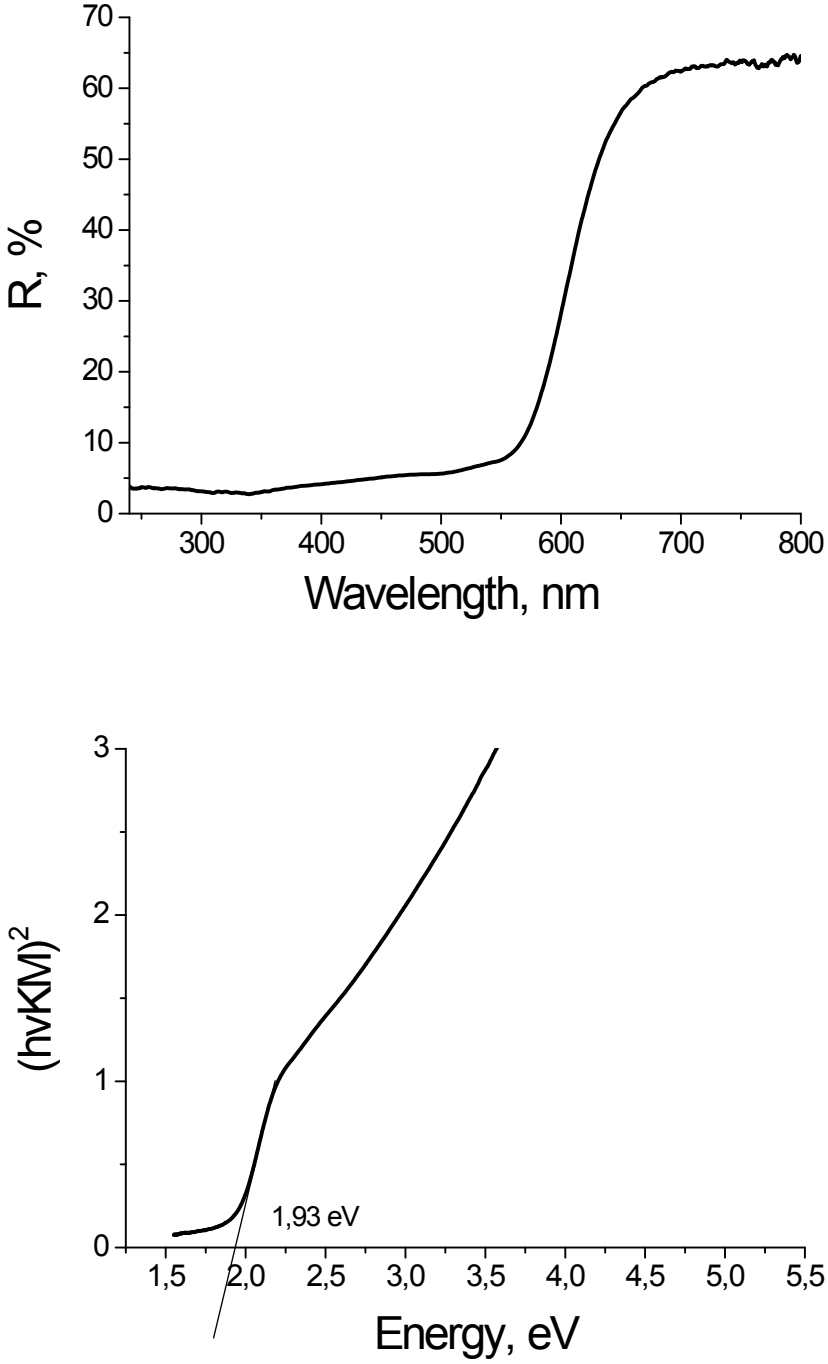

Figure 12S. Diffuse reflectance spectrum (above) and dependence of $(h\nu KM)^2$ (below) on the incident radiation energy for **6**

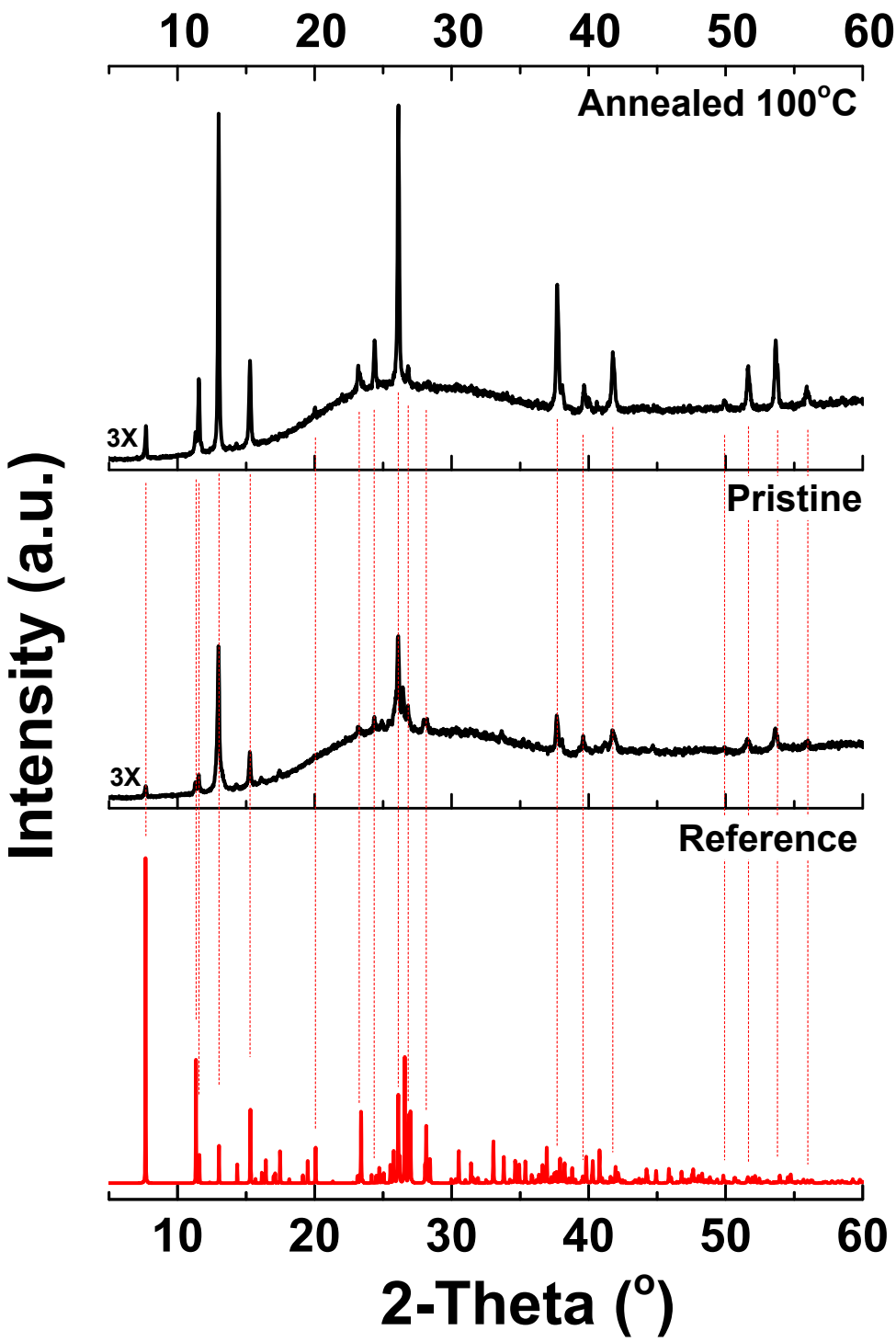

Figure 13S. XRD patterns for as-deposited thin film of **1** and annealed at 100°C for 10 minutes compared to the reference pattern simulated from the single-crystal x-ray data for **1**.

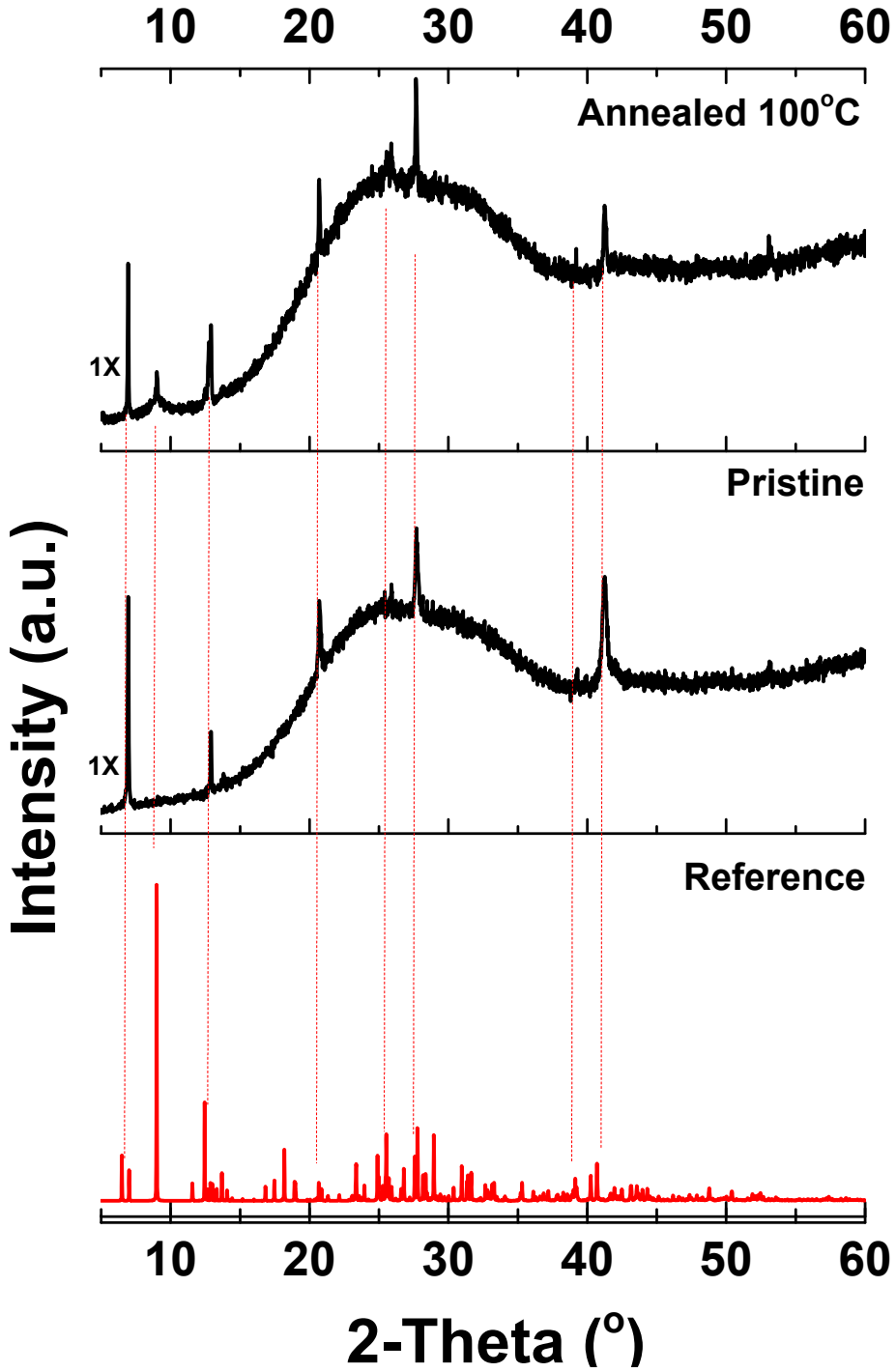

Figure 14S. XRD patterns for as-deposited film of **3** and annealed at 100°C for 10 minutes compared to the reference pattern simulated from the single-crystal x-ray data for **3**.

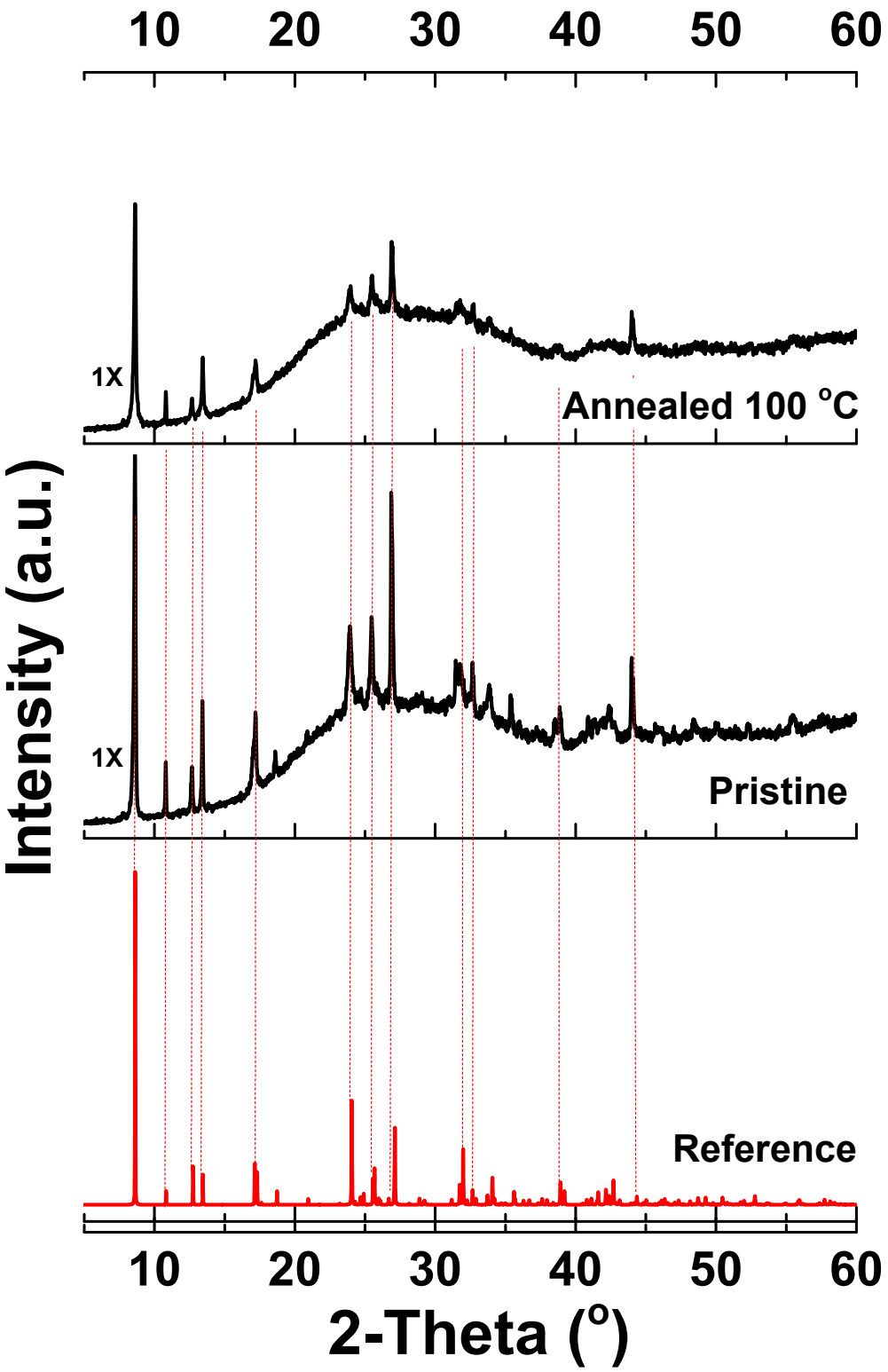

Figure 15S. XRD patterns for as-deposited film of **5** and annealed at 100°C for 10 minutes compared to the reference pattern simulated from the single-crystal x-ray data for **5**.

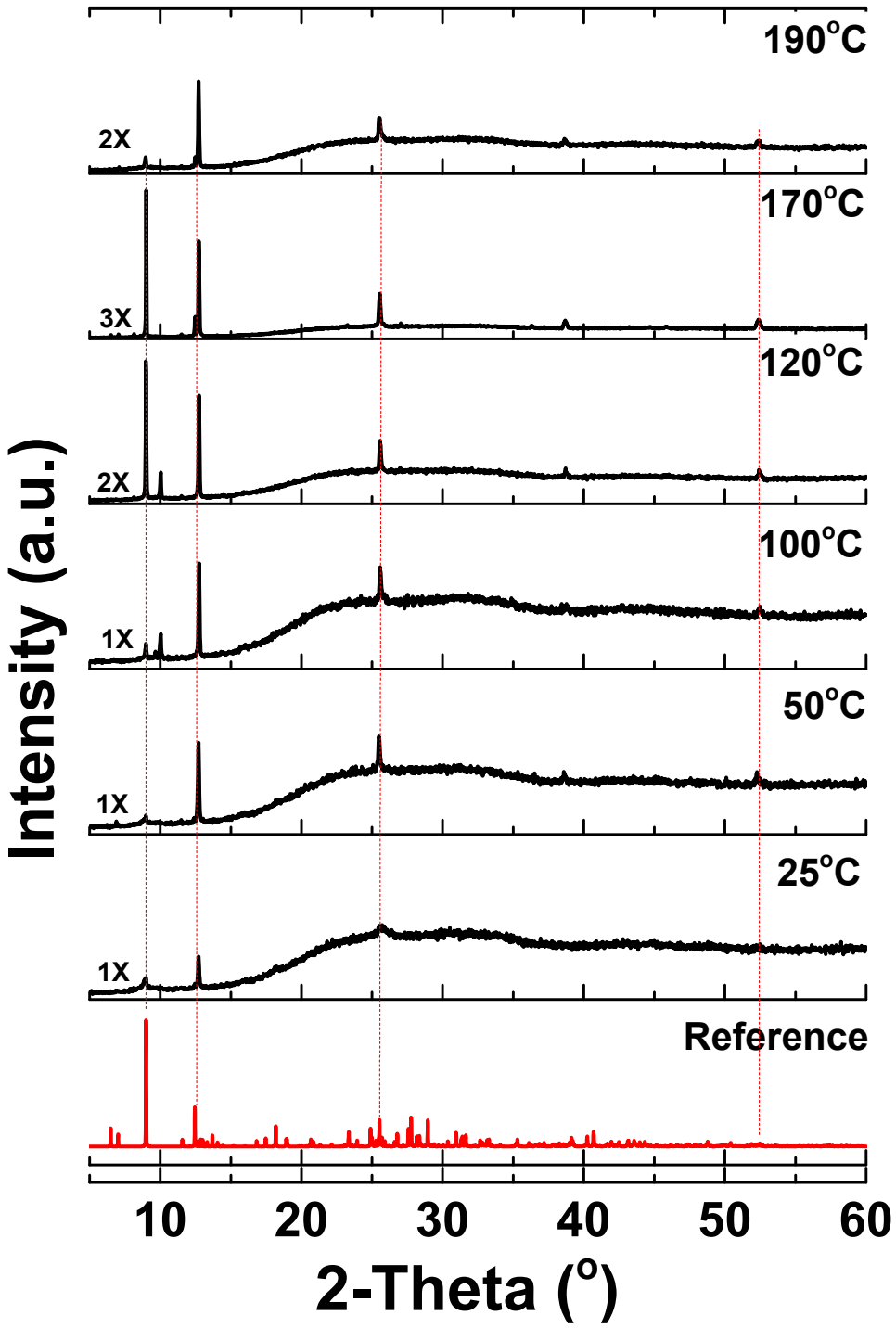

Figure 16S. Evolution of the XRD patterns of thin film of **3** as a function of the annealing temperature. The reference XRD pattern simulated the single-crystal x-ray data for this compound is given for comparison.

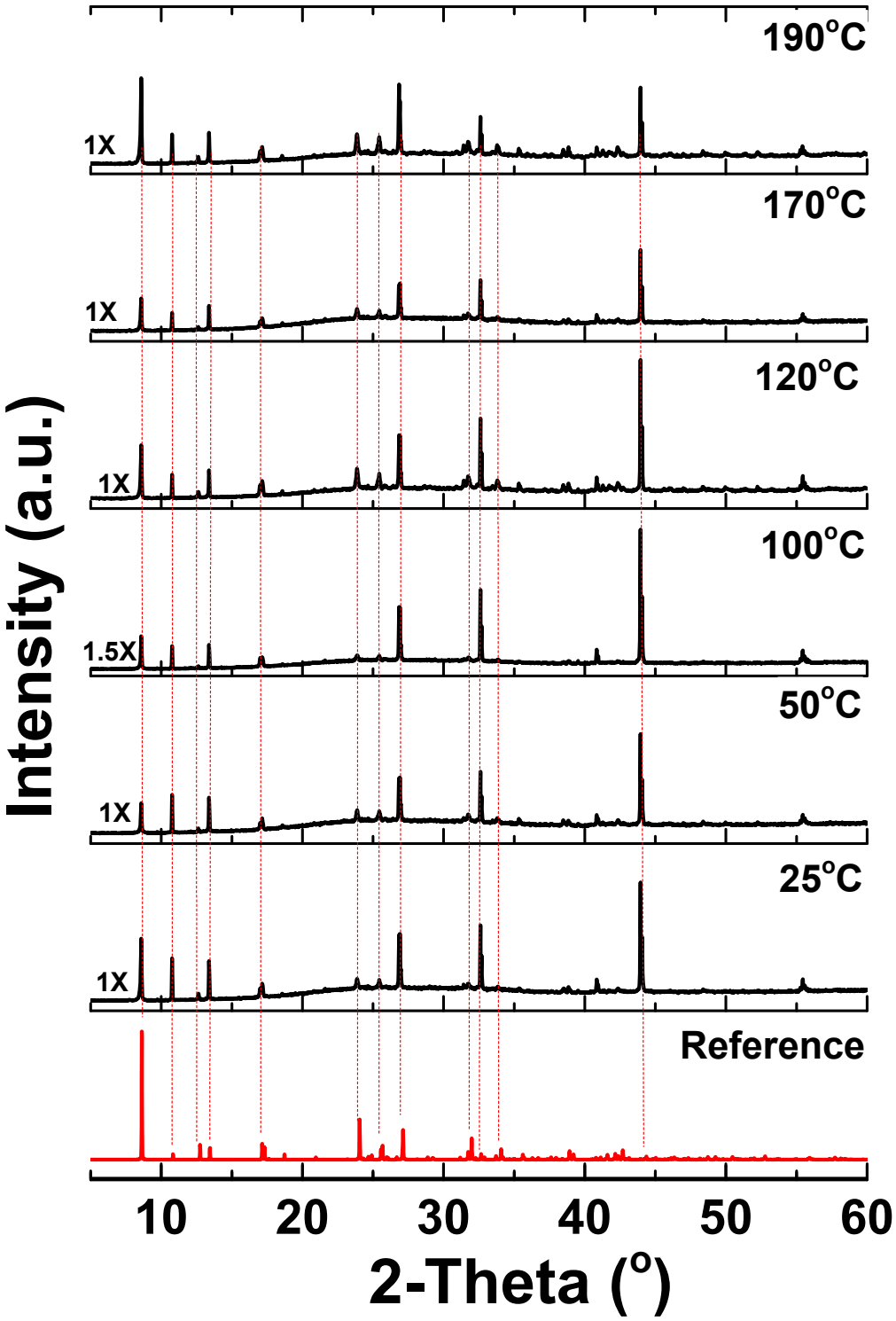

Figure 17S. Evolution of the XRD pattern of thin film of **5** induced by thermal annealing. Experimental XRD profile of BiI_3 and the pattern simulated from single-crystal x-ray data for **5** are given for comparison.

a)

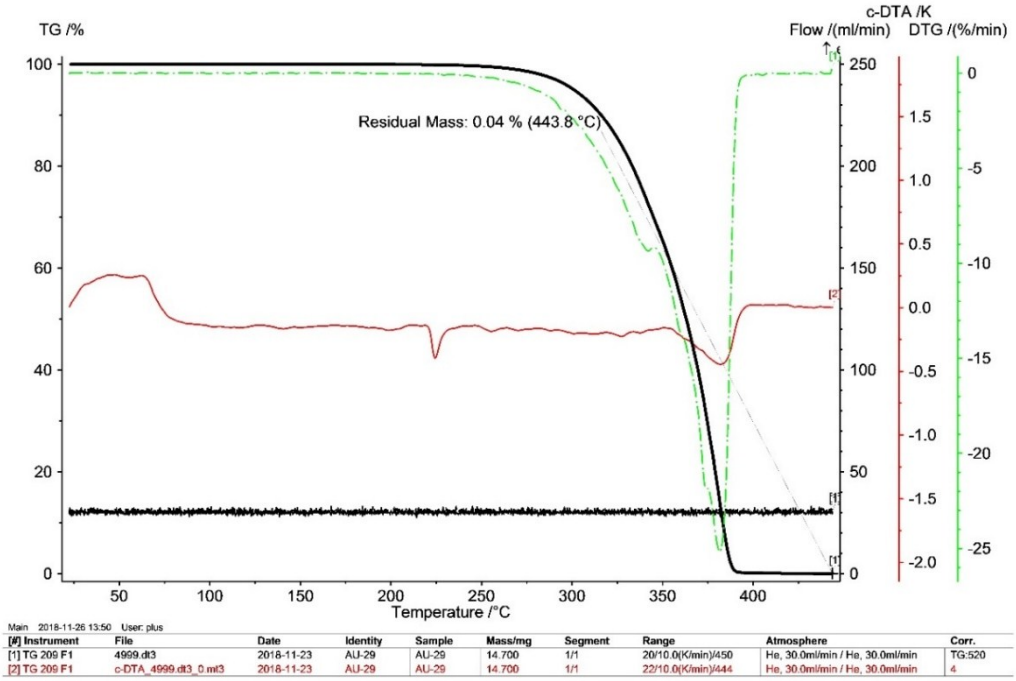

b)

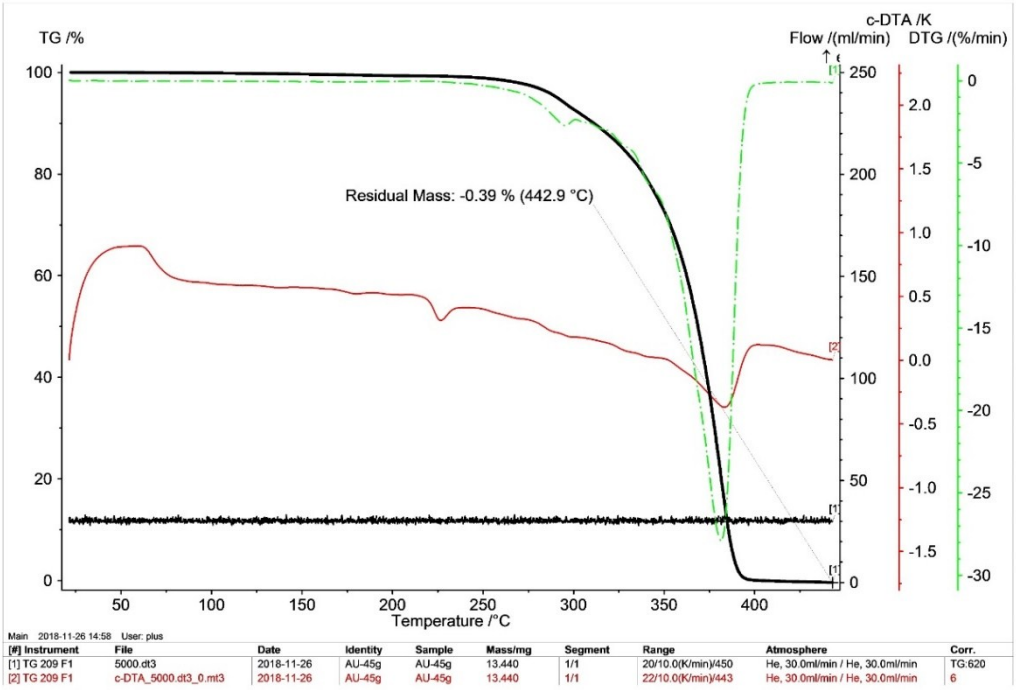

Figure 18S. TGA curves for N-MePy[Bi_3I_{10}] **1** (a) and N-MePy[Bi_2I_3] **2** (b)

a)

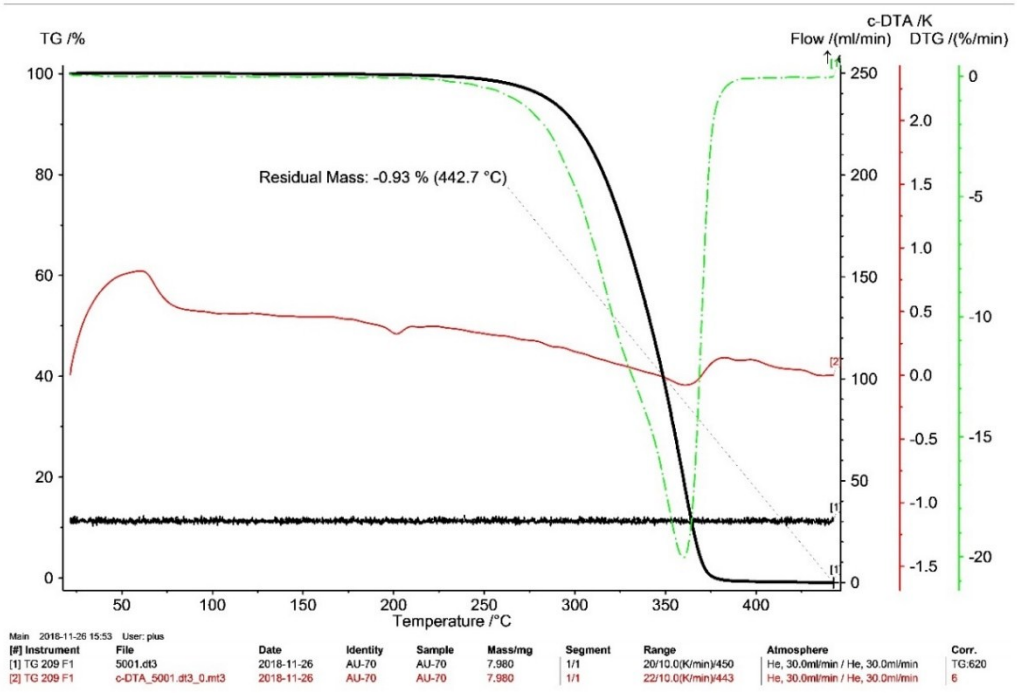

b)

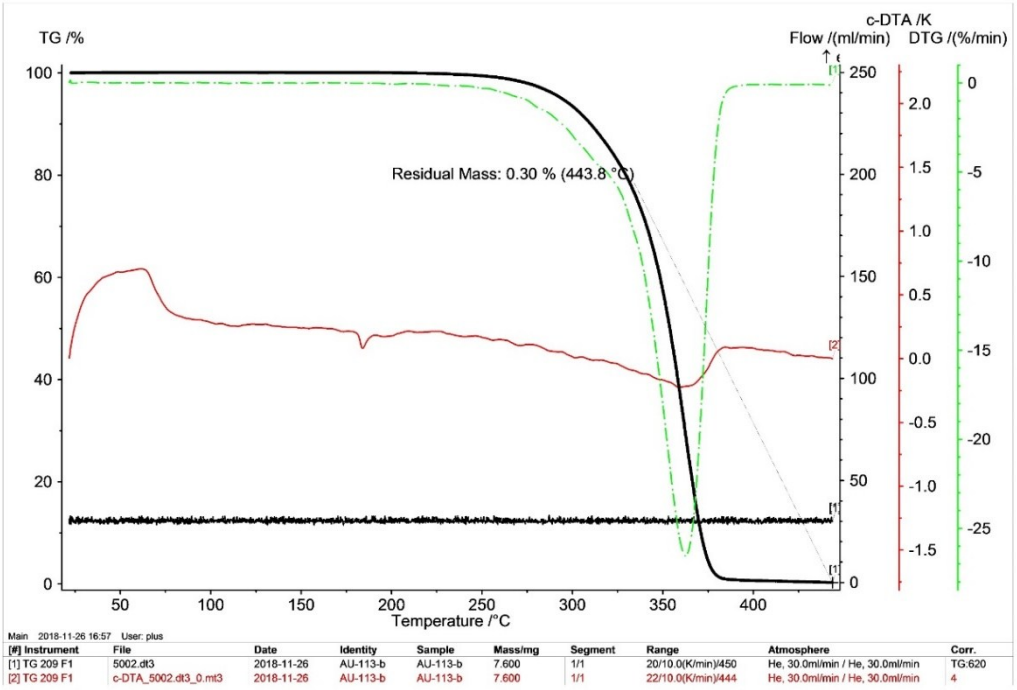

Figure 19S. TGA curves for N-EtPy[Bi_3I_{10}] **3** (a) and N-EtPy[Bi_2I_3] **4** (b).

a)

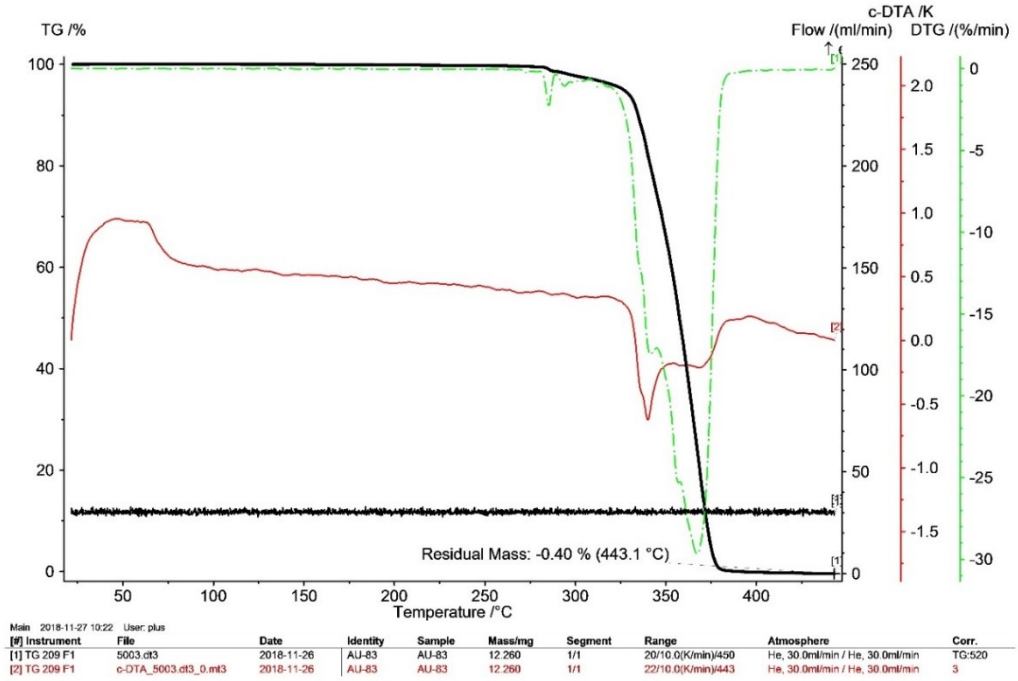

b)

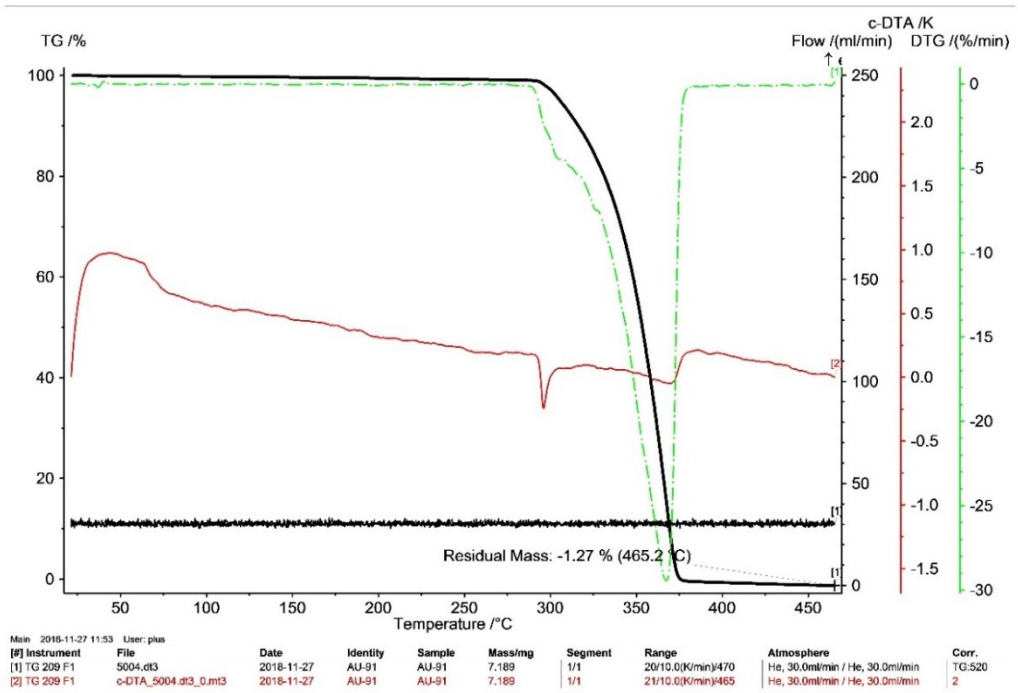

Figure 20S. TGA curves for N-methyl quinolinium[BiI_4] **5** (a) and N-methyl isoquinolinium[BiI_4] **6** (b)

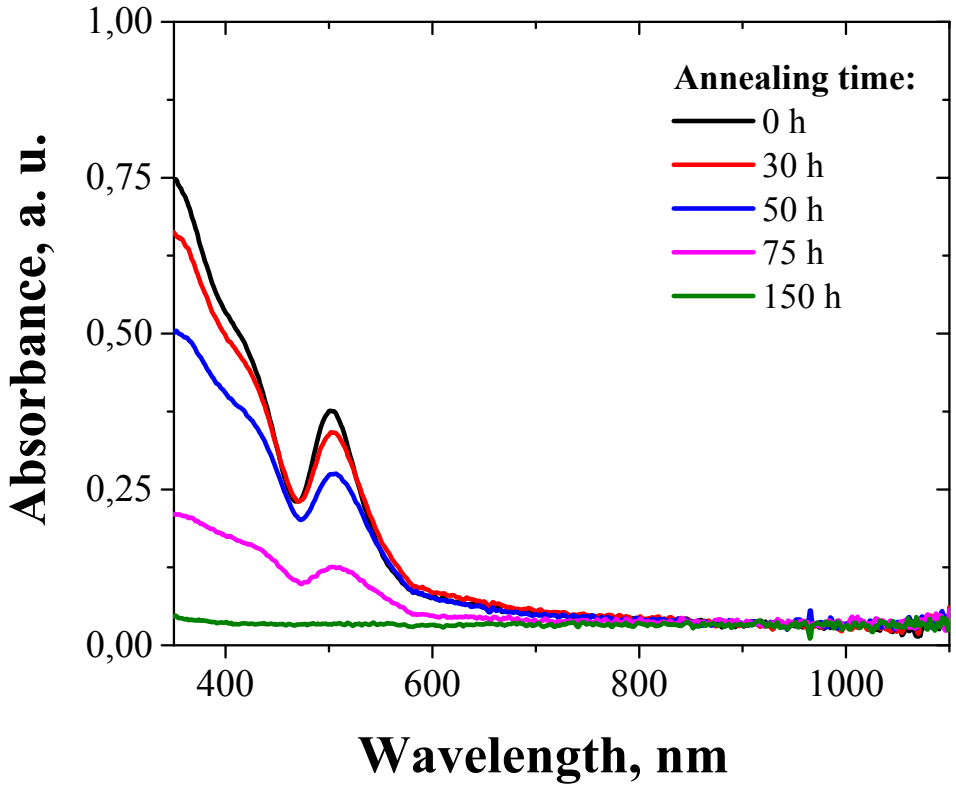

Figure 21S. Evolution of the absorption spectra of thin film of $MA_3Bi_2I_9$ during continuous thermal annealing at 65-70 °C showing its rapid decomposition within less than 150 h.

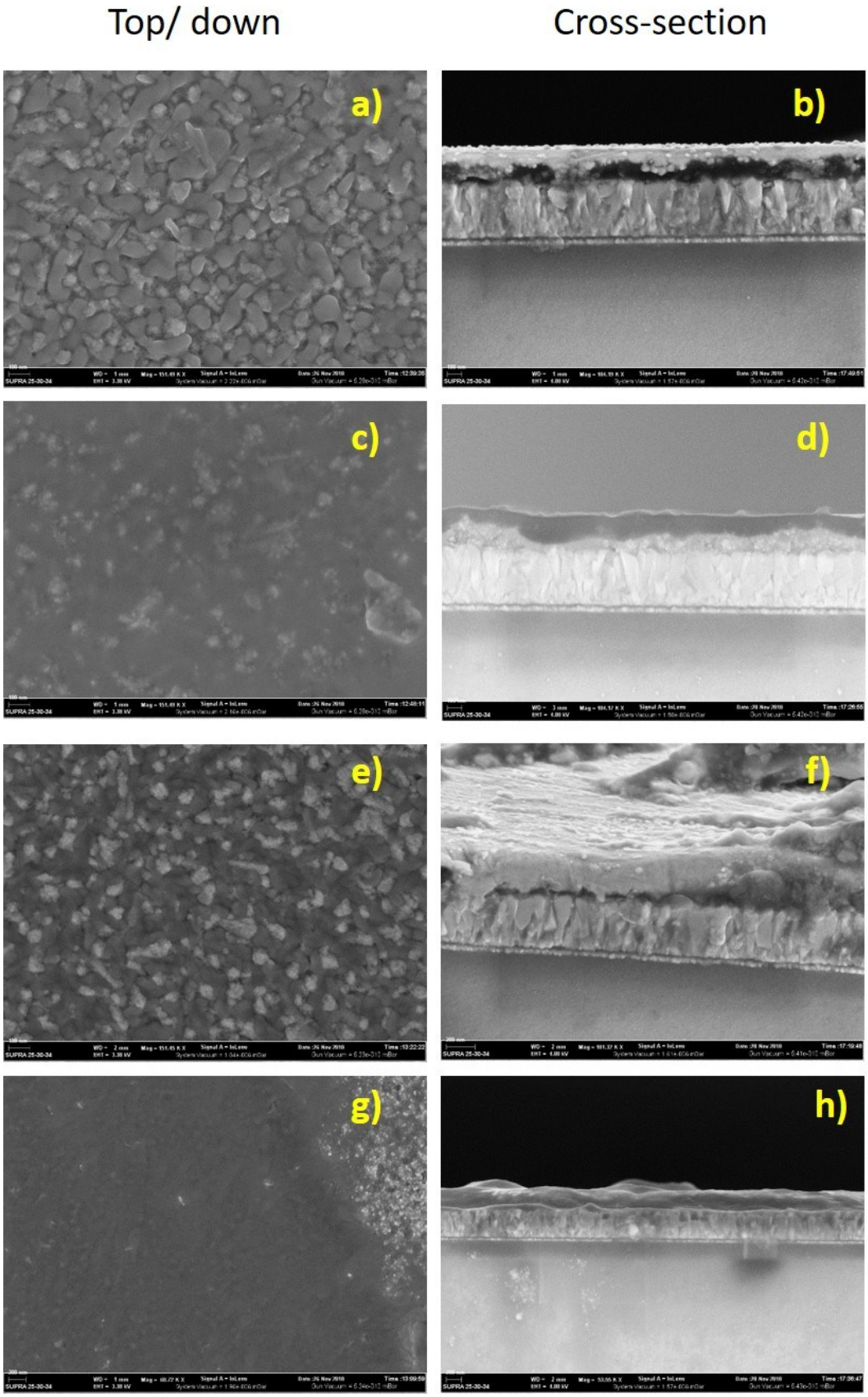

Figure 22S. Top-view and cross-sectional SEM images of **1** (a, b), **3** (c, d), **5** (e, f) and **6** (g, h) films deposited on conductive FTO/TiO_2 substrates

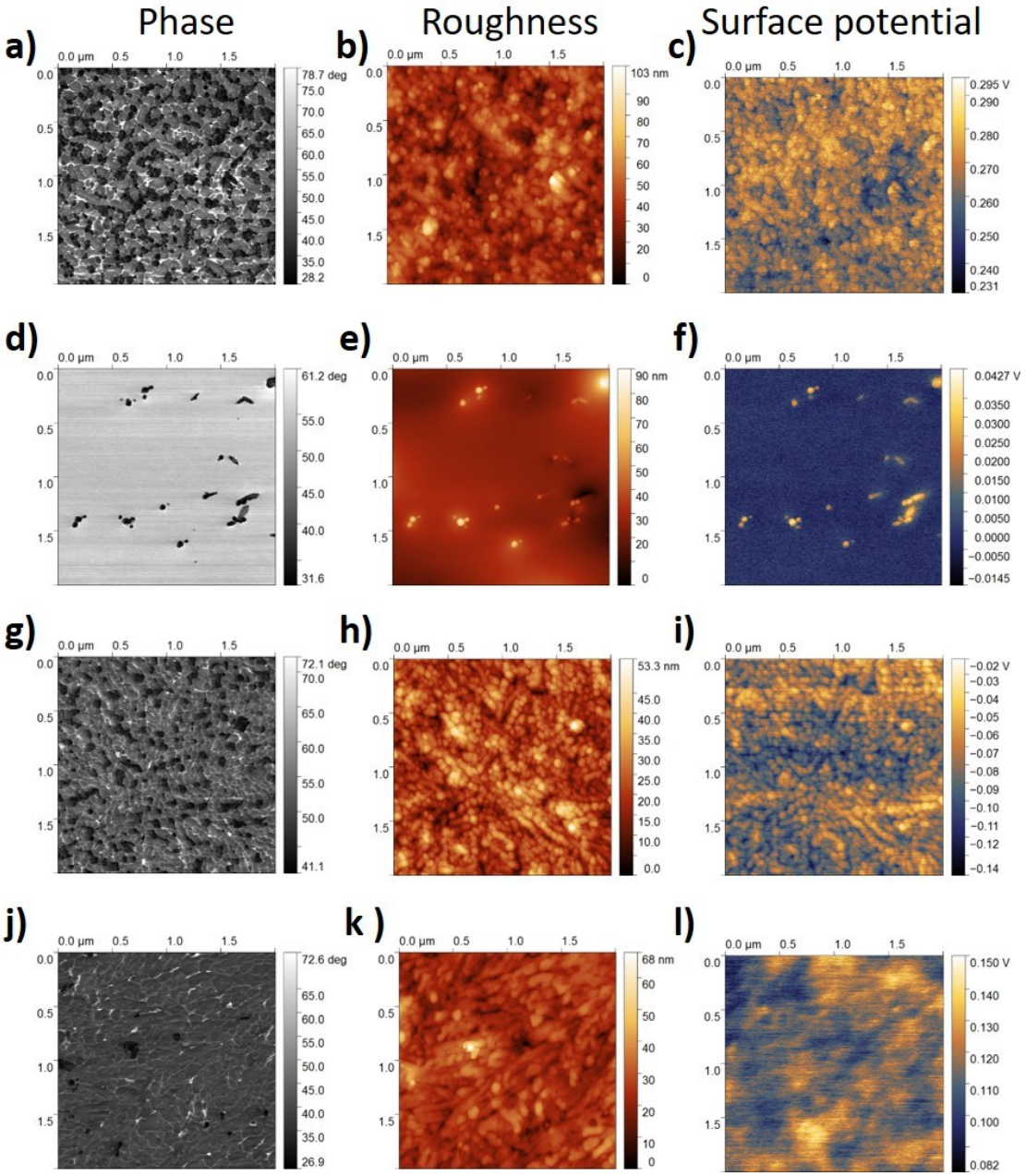

Figure 23S. Phase (left), surface topography (middle) and surface potential (right) images of **1** (a, b, c), **3** (d, e, f), **5** (g, h, i) and **6** (j, k, l) films deposited on conductive FTO/TiO_2 substrates

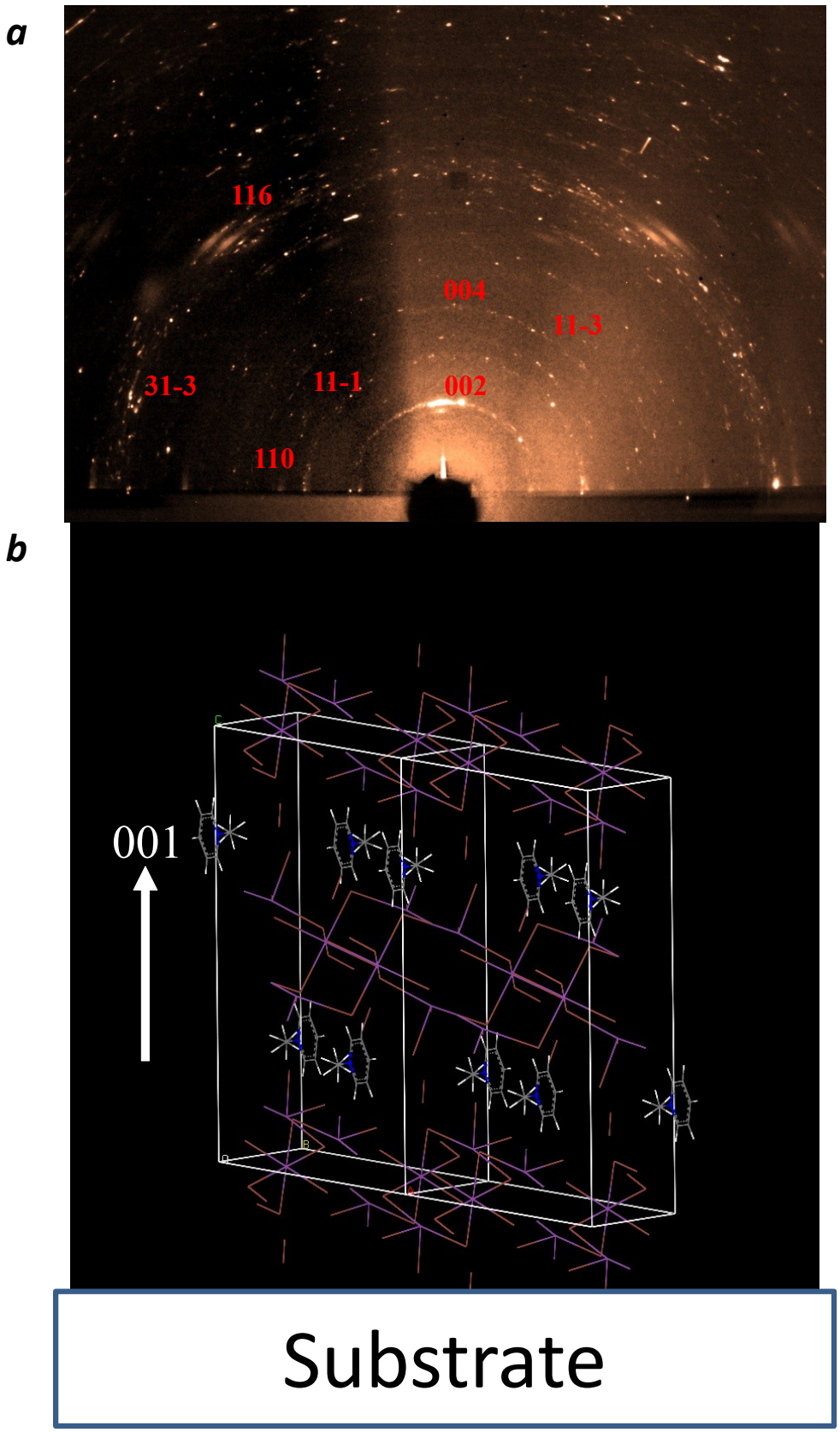

Figure 24S. Experimental 2D GIXRD profile of thin film of **1** (a) and orientation of the Bi-I molecular frameworks with respect to the horizontal substrate (b)

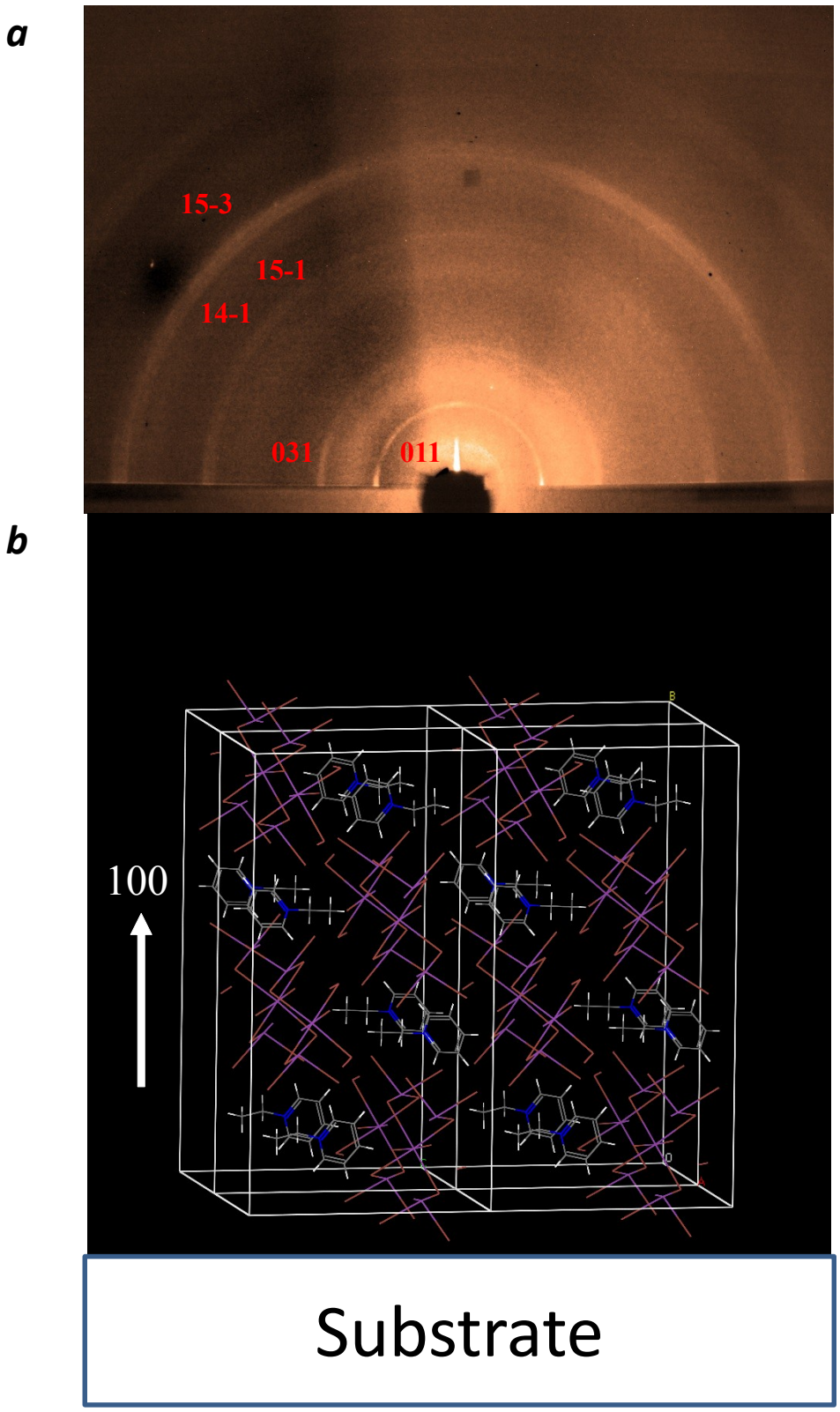

Figure 25S. Experimental 2D GIXRD profile of thin film of **3** (a) and orientation of the Bi-I molecular frameworks with respect to the horizontal substrate (b)

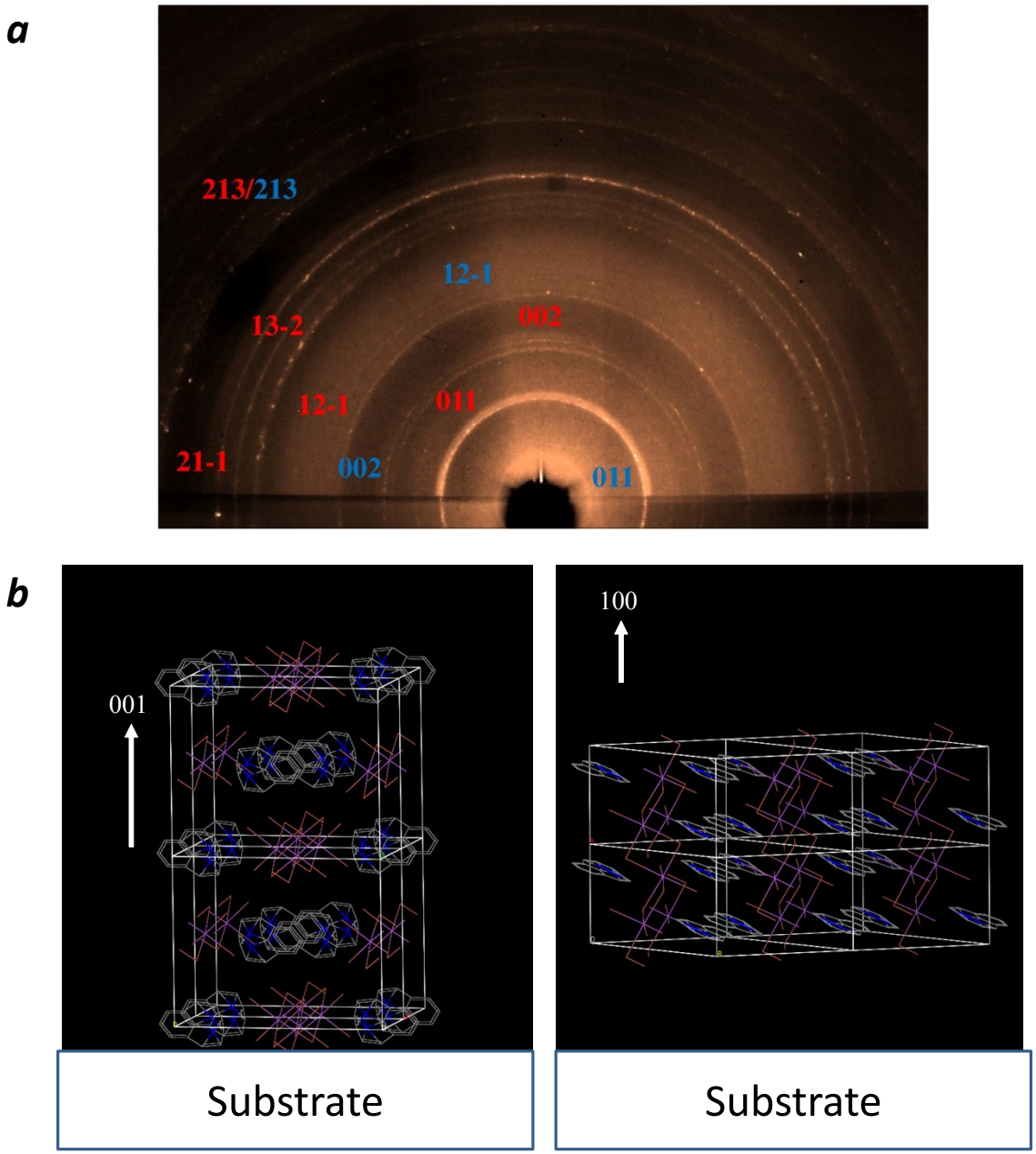

Figure 26S. Experimental 2D GIXRD profile of thin film of **5** showing reflexes of crystalline domains with horizontal (red color) and vertical (blue color) orientation of Bi-I chains (a). Projections of unit cells with the horizontal (left) and vertical (right) orientations of the Bi-I molecular frameworks with respect to the horizontal substrate (b).

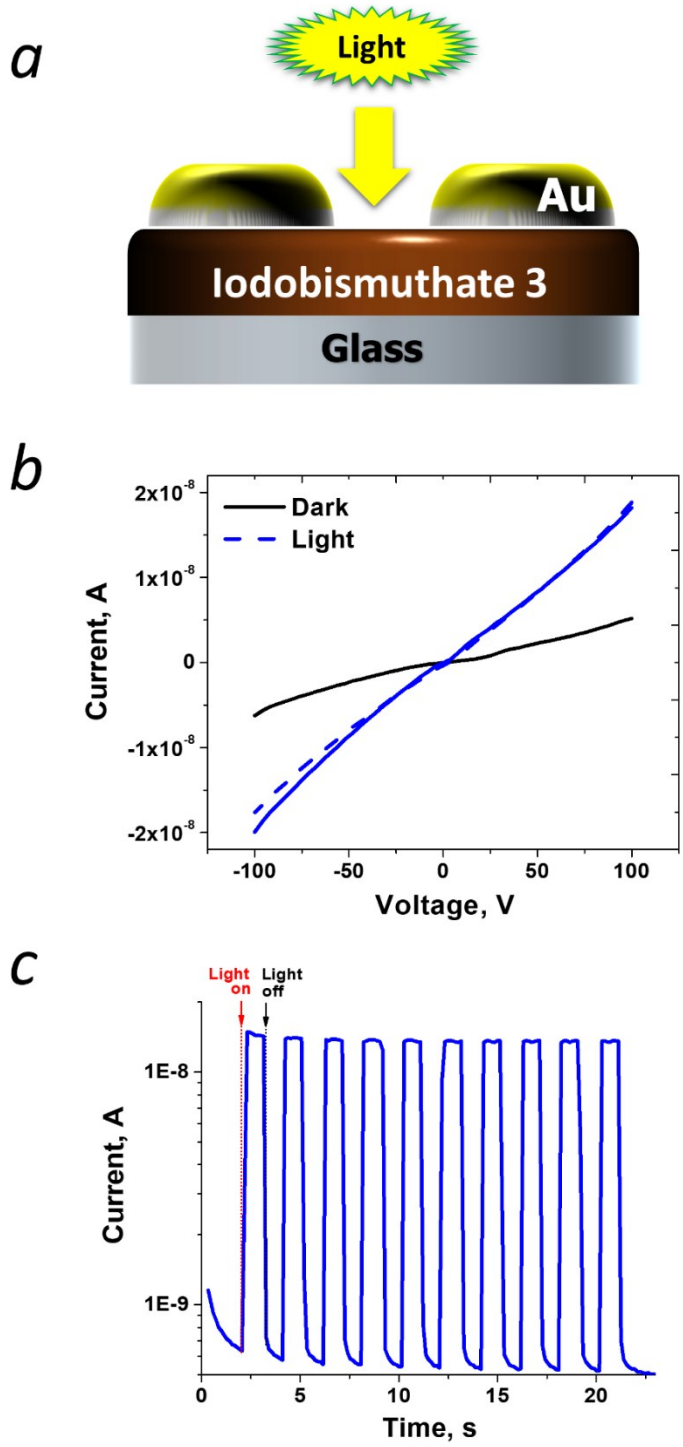

Figure 27S. A schematic layout of the lateral device with thin film of **3** (a). Current–voltage characteristics of the lateral diodes with the photoactive films of **3** measured in dark and under illumination (violet laser, λ=405 nm, 70 mW/cm^2) in the forward (solid lines) and reverse (dashed lines) directions (b). Light-induced switching of the devices at the bias voltage of 100V (c).

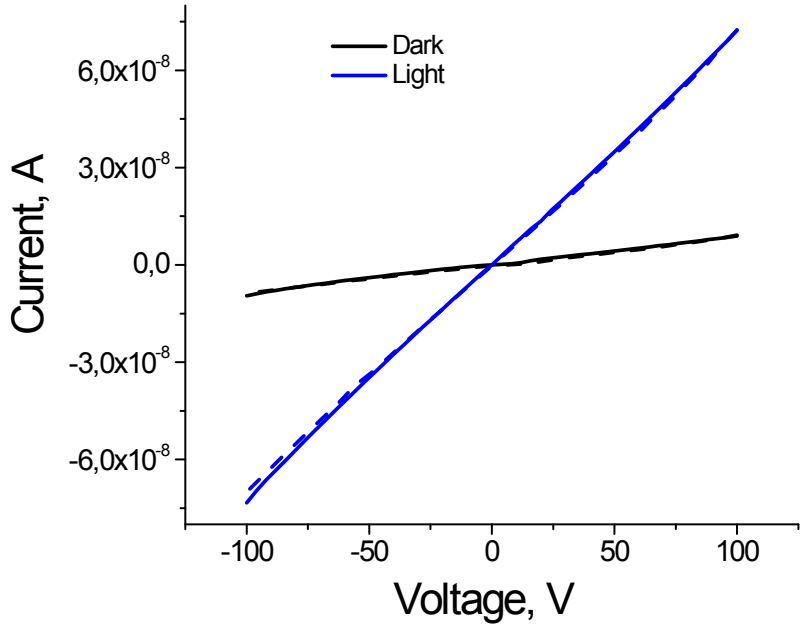

Figure 28S. Current–voltage characteristics of the lateral diodes with the photoactive films of fullerene C_{60} (100 nm) measured in dark and under illumination (violet laser, λ=405 nm, 70 mW/cm^2) in the forward (solid lines) and reverse (dashed lines) directions

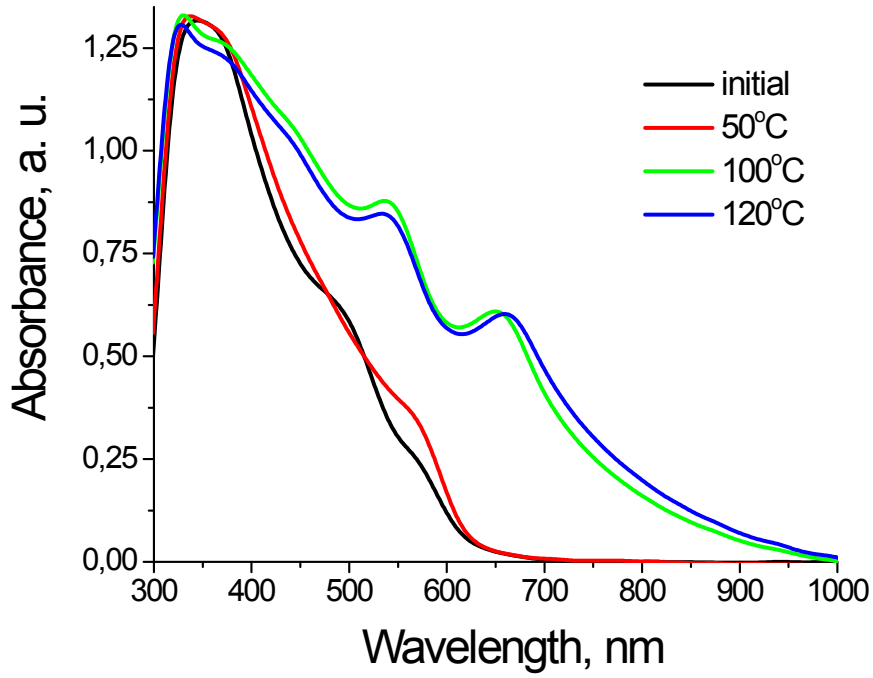

Figure 29S. Evolution of the absorption spectra of **3+I$_2$** films under thermal annealing

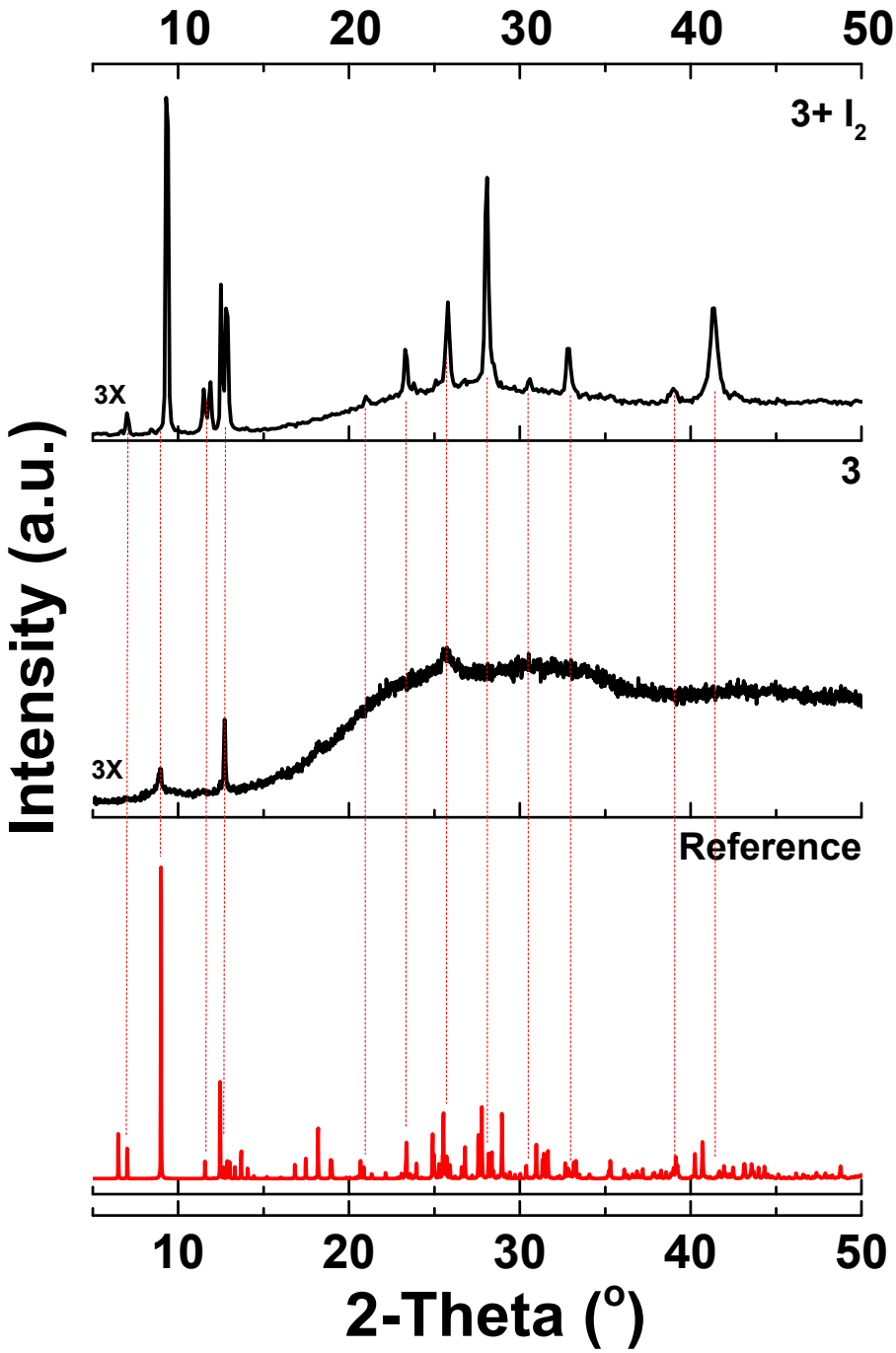

Figure 30S. XRD patterns of **3** and **3+I_2** systems; the reference pattern for **3** simulated from x-ray single crystal data is shown for comparison